2002

Assessment of the impact of camshaft machining inputs on valve train sound quality using vibration analysis.

Matthew C. Daws
University of Windsor

ASSESSMENT OF THE IMPACT OF CAMSHAFT MACHINING INPUTS ON VALVE TRAIN SOUND QUALITY USING VIBRATION ANALYSIS

by

Matthew C. Daws

A Thesis
Submitted to the Faculty of Graduate Studies and Research
through the Department of Mechanical, Automotive and Materials Engineering
in Partial Fulfillment of the Requirements for
the Degree of Master of Applied Science at the
University of Windsor

Windsor, Ontario, Canada
2002

ABSTRACT

A study was undertaken to investigate the dependence of valve train sound quality on certain camshaft machining parameters. In particular, a sound quality issue referred to as *camshaft chatter* was investigated. Camshaft chatter refers to a noise caused by geometrical undulations on the camshaft lobes that excite valve train and cylinder head vibration modes during operation. The undulations are an artifact of the manufacturing process.

The engine used in the study was a dual overhead camshaft (DOHC) V6. Eight different left-hand-side exhaust camshafts were manufactured with different, known combinations of the selected machining parameters. Each parameter was varied between a "high" and "low" setting.

Tri-axial accelerometers were mounted at two locations on the cylinder head of the test engine, and extensive vibration data was collected for each camshaft.

The vibration data was analyzed using a number of methods, including: time domain analysis, RMS analysis, angle domain variance analysis, and RPM-frequency analysis.

After a method was developed to objectively quantify the severity of camshaft chatter, a main effects analysis was performed to assess the impact of the individual machining inputs.

It was found that vibration of the camshaft grinding wheel had the largest impact on camshaft chatter, followed by vibration of the grinding wheel motor. Tension of the drive belt was also shown to impact the severity of the chatter phenomenon.

DEDICATION

This work is dedicated to my girlfriend Jamie who has stood by my side throughout my entire university experience and has offered unrelenting support, understanding, and encouragement. This work is also dedicated to my parents, whose financial support, encouragement, and words of praise made everything possible.

ACKNOWLEDGEMENTS

The author would like to express his appreciation first and foremost to Dr. Jimi Tjong for providing the equipment and facilities for this study. This thesis would not have been possible without the continuing support and patience of Dr. Tjong.

Special thanks go out to Dr. G. Reader, Dr. M. Ahmadi, Dr. N. Zamani, and Dr. G. Rankin for assuming committee roles.

Collection of the data would not have been possible without the continued assistance of the dynamometer technicians employed under Dr. Tjong. In particular, the author would like to thank Mr. R. Ellwood, Mr. R. Koresky, and Mr. T. Murawski.

Thanks to Dr. B. Seth, Mr. J. DeVerna, and Mr. J. Glowa for providing the camshafts and other related information used in this study.

TABLE OF CONTENTS

LIST OF TABLES

TABLE

LIST OF FIGURES

FIGURE

NOMENCLATURE

A	amplitude of displacement response
AC	Alternating Current
ADC	Analog-to-Digital Converter
$ATDC$	After Top Dead Center
$a(t)$	vibration acceleration response
BDC	Bottom Dead Center
$BTDC$	Before Top Dead Center
c	damping co-efficient
c_{cr}	critical damping co-efficient
CI	Compression Ignition
CID	Camshaft Identification signal
CPS	Crankshaft Position Sensor
DC	Direct Current
$DOHC$	Dual Over Head Camshaft
ΔA_{sig}	smallest resolvable change in signal amplitude
Δf	frequency resolution
Δt	time spacing of samples
F	force
FFT	Fast Fourier Transform
FS	full-scale voltage range of analog/digital converter
f	frequency in Hz
f_c	force due to damper acting on mass
f_k	force due to spring acting on mass
f_{max}	maximum frequency of interest
F_s	sampling rate
g	acceleration due to gravity
$G_{yy}(f)$	one-sided autopower spectrum
i	index for data points
k	spring constant
m	mass in lumped parameter system
n	general counter variable
N	engine rotational speed (RPM)
NL	No-Load / Neutral
NVH	Noise, Vibrations, and Harshness
OHC	Over Head Camshaft
P	power output
PT	Part Throttle
r	radius
RPM	Rotations Per Minute
RMS	Root Mean Square
RV_i	Running Variance of i^{th} position in angle domain
SI	Spark Ignition

S_{yy}	autopower spectrum of signal $y(t)$
$SOHC$	Single Overhead Camshaft
σ_i	variance of i^{th} position in angle domain
θ	crankshaft angle
t	time in seconds
T	length of measurement period
TTL	Transistor-Transistor Logic
$v(t)$	vibration velocity response
v_0	initial value of velocity
WOT	Wide-Open Throttle
$x(t)$	vibration displacement response
x_0	initial value of displacement
X_{RMS}	signal RMS value
$\bar{y}(t_i)$	linear average of signal $y(t)$ at i^{th} point in time record
$y(t)$	general continuous time-domain function
$y(t_k)$	general discrete time-domain function
$Y(f)$	general frequency-domain function
$Y^*(f)$	complex conjugate of frequency-domain function
$Y(k)$	general discrete frequency-domain function
ϕ	phase of displacement response
$\lambda_{1,2}$	roots of characteristic equation
ω	undamped natural frequency of spring-mass-damper system
ω_d	damped natural frequency of spring-mass-damper system
$\overline{X}_{A+}$	average response when factor A is set to HIGH
$\overline{X}_{A-}$	average response when factor A is set to LOW
ζ	damping ratio

CHAPTER 1

INTRODUCTION

The powertrains of modern passenger cars are expected to meet many demands: not only are adequate power and low engine-speed torque expected, but also improved response and "smoothness" are desired. In addition, low fuel consumption and reduced exhaust emissions must be achieved to address environmental concerns.

Due to the ever-increasing customer expectations regarding "smoothness" of automobile operation, the field of Noise, Vibrations, and Harshness (NVH) has received more attention in recent years than it has in the past.

Harshness is the branch of NVH that addresses the subjective aspects of noise and vibrations. Identification of the portions of a particular sound or vibration event that are either annoying or preferable to customer perception is a key issue in the design process of modern automobiles. In general, if a noise is concentrated in a narrow bandwidth, or has a very rapid rise time, or is intermittent or irregular, it is deemed "noisier" than if it remains steady [15]. Words like "rattle", "croak", "chirp", "hiss", "clunk", and "chatter" are often used to describe customer complaints related to noise and vibrations. Addressing such issues is a challenge for the powertrain development engineer, because the complaints are highly subjective in nature. Evaluations are often made using subjective rating systems by groups of experienced listeners. Once system sounds are identified and annoyance levels are determined, a correlation study is performed to attempt to find objective measurements that can quantify customer perception of a particular noise or vibration event. These measures can then quantify any subsequent hardware modifications in terms of their effects on perceived sound quality.

This study was performed to address a sound quality (i.e. harshness) issue associated with the camshaft of a dual overhead cam (DOHC) V6 engine. The complaint, which will hereinafter be referred to as "camshaft chatter", was dependent on various aspects of the camshaft manufacturing process. The objectives for this study were as follows:

1. To carry out engine vibration tests using a number of different specially-made camshafts – each with different combinations of manufacturing parameters.
2. To verify that the camshaft chatter phenomenon is manifested in the acquired data.
3. To find a means of quantifying the severity of the camshaft chatter in each case.
4. To assess the impact of each of the chosen manufacturing inputs on the severity of camshaft chatter.

CHAPTER 2

LITERATURE SURVEY

2.1 Noise and Vibration in Internal Combustion Engines

Noise and vibration are intimately related. In fact, vibration is often the origin of noise. Almost all practical dynamic mechanical systems vibrate during operation, so it is very reasonable to suppose that noise and vibration signals may be used as a basis for fault diagnosis and condition monitoring. Observation of the noise and vibration generated by internal combustion engines is of interest because it provides a rapid means of monitoring the condition of the engine without having to resort to disassembly. The information obtained from the analysis may be used to detect abnormal operating conditions, to estimate the severity of the abnormality and, in many cases, to determine the source of the abnormality.

2.1.1 Engine Noise

When dealing with automotive engines, *noise* may be defined as any sound that is undesirable to the customer. In general, any sound emitted from an engine is undesired, therefore, all sound emitted from an engine shall be referred to as noise. Engine noise may be divided into three main categories [24]:

1. *Fluid Flow Noise* – noise caused by the induction of air, the expulsion of exhaust gases, and the flow of other fluids within the engine such as oil and coolant.
2. *Combustion Noise* – noise caused by rapid pressure rise in engine cylinders during combustion, and combustion knock.

3. *Mechanical Noise* – noise caused by the interaction of, or the impact between, the moving components of an engine.

Since this study deals strictly with the detection and analysis of engine mechanical phenomena, fluid flow noise and combustion noise are considered to be outside the scope of this thesis and will not be given further consideration.

Mechanical noise originates, to varying degrees, from all moving parts within an engine. It encompasses the noise that originates due to the vibrations produced by the physical interaction of two or more engine components [21]. Sources of mechanical noise include (but are not limited to): piston slap, excessive bearing clearances, gear meshing, timing drives, valve train impacts, and fuel injectors.

2.1.2 Engine Vibration

Vibration may be defined as the oscillatory motion of an object or surface relative to a stationary frame of reference. Engine vibration is universally considered to be undesirable. From a vehicle owner's standpoint, engine vibration is intrusive and annoying. From a design standpoint, excessive vibration may lead to the premature failure of engine components [17]. The causes of engine vibration may be divided into the following categories:

1. *Unbalanced Forces* – static and dynamic unbalance of rotating parts, piston unbalance, etc.
2. *Elastic Reaction* - bending of the crankshaft and crankcase due to centrifugal forces that may be equal but are in different planes, downward deflection of the crankshaft

due to combustion forces, and torsional displacement of the crankshaft due to uneven turning effort

3. *Mechanical Interaction* – the physical impact between two or more engine components causing kinetic energy to be converted to vibration energy
4. *Combustion* – pressure waves originating from combustion processes impacting the cylinder walls

Vibration due to unbalanced forces and elastic reactions is generally minimized at the design stage in modern engines through the use of counter-balancing, torsional damping, and cancellation techniques.

2.1.2.1 Valve Train Excitations in Overhead Camshaft Engines

Vibrations originating in the valve train of an overhead camshaft (OHC) engine are caused during the following three events [36]:

1. *Valve opening* – During this period, the rotating camshaft lobe moves the valve train components (tappet, spring retainer, and valve) against the resistance of the valve spring. Harmonics of the cam profile and undulations on the camshaft lobe excite valve train and cylinder head vibration modes.
2. *Valve closing* – During this period, the force exerted on the valve train components by the compressed valve spring forces the valve train components against the camshaft lobe. The camshaft lobe thus serves to *constrain* the motion of the components.
3. *Valve seating* – This event corresponds to the moment the valve head comes into contact with the valve seat. Valve seating is a typical example of a mechanical

impact event. The kinetic energy of the valve train components is converted into the vibration energy of the surrounding structure, and heat.

2.2 Acquiring Engine Noise and Vibration Data

In order to obtain the noise and vibration data needed to assess the condition of an engine, an adequate testing system must be designed. The design of a measurement system consists of: selection of an appropriate technique, selection of suitable instruments, proper calibration or system verification tests, and a well-thought-out plan on how the measurement data are to be handled, reduced, and interpreted [1].

2.2.1 Data Acquisition Systems

Modern data acquisition equipment forms a very broad spectrum of sophistication and versatility. The choice of equipment is mainly dictated by the goals of the associated testing, but other factors such as availability, size, durability, and resistance to extreme conditions will have an influence as well [2]. In some cases, a single-channel analog oscilloscope that displays time-based waveforms may be all that is necessary to extract the desired information. Multi-channel digital storage oscilloscopes and dynamic signal analyzers offer more advanced features, such as the ability to calculate real-time frequency spectra and store data to disk for post-processing. In general, however, the highest level of flexibility is afforded by computer-based (i.e. PC or Unix) data acquisition systems. Such systems typically comprise high-speed, high-resolution (12 bits or more), multi-channel analog to digital converters (ADC) and user-friendly software that allows the user to configure the data acquisition to suit his or her needs [8].

As well, some systems provide data processing capabilities. Figliola and Beasley [1] and Wheeler and Ganji [2] discuss various important data acquisition methods and considerations.

2.2.2 Transducers

Transducers are devices that convert physical phenomena into measurable signals. When performing measurements, it is important to choose transducers that are suitable for the specific application. In particular, the valid frequency range of the transducer should encompass the frequencies that are of interest in the measurement. Other factors that will influence the choice of transducer include the required accuracy, the required precision, and size constraints. The temperature of the test environment, the presence of contaminants such as dirt and oil, and the presence of electrical noise sources such as power lines should also be considered. A discussion of the various transducers that are used in modern engineering measurements may be found in Figliola and Beasley [1] and Wheeler and Ganji [2].

2.2.2.1 Transducers for Measurement of Engine Vibration

The piezoelectric accelerometer is the most commonly used type of transducer for vibration measurements because it is durable, inexpensive, relatively small, and it has a broad frequency range. Accelerometers are ideal for measurements on engines because with little effort they can be mounted at numerous locations and, due to their small mass compared to the engine, their presence does not affect the vibration. Accelerometers generate analog signals that are proportional to the acceleration of the surface to which

they are attached. It is important to note, however, that accelerometers only provide information about a single point on the surface. Serridge and Licht [30] offer a comprehensive reference on the construction and use of piezoelectric accelerometers.

Vibration transducers that employ laser doppler technology (see, for example, Forbes et al [12]) to measure velocity have the advantage that they are non-contact sensors that may be used to scan the surface of the engine thus providing data for numerous locations.

2.2.3 Measurement Environment

When performing any kind of measurement, it is important to understand the characteristics of the environment that may affect the results. The following sections discuss the main environmental factors that should be considered when performing engine vibration measurements.

2.2.3.1 Factors Affecting Measurement of Vibration

Due to the widespread use of accelerometers for vibration studies, the information obtained is usually associated with a single point on a surface. Still, vibrations originating from all parts of the engine propagate through the structure and affect the results obtained from any particular point of interest. Inman [26] provides an in-depth discussion of vibration theory, modeling, and measurement.

As stated by Serridge and Licht [30], it should be noted that the following factors can affect vibration measurements when using piezoelectric accelerometers: extreme

temperatures, temperature transients, extreme sound pressure levels, humidity, magnetic fields, and gamma radiation.

When measuring engine vibrations, the engine is usually resting on a rigid steel palette, firmly attached to mounts, or installed in an actual vehicle. If, for example, the engine is mounted on a dynamometer test stand in a laboratory, the vibration characteristics of the engine will differ from those observed when the engine is installed in a vehicle [19]. This phenomenon will be observed if the mount stiffness characteristics of the laboratory facilities are not the same as those found in the vehicle. Differing mount stiffness characteristics cause varying amounts of vibration energy to be transmitted to the surroundings (i.e. vehicle body or test stand).

2.2.4 Positioning of Transducers

In order to maximize the useful information that is obtained from a measurement, and minimize the presence of unwanted signal noise and interference, due consideration should be given to the positioning of the transducers and, in the case of contact sensors, the condition of the measurement surface.

An understanding of the vibration mode shapes of the engine being studied helps to reveal where the measurements should be taken in order to obtain the strongest signal. Ewins [3] is an example of a reference that provides a detailed discussion of modal analysis. In many cases, a trial-and-error approach may be necessary to determine the measurement locations that provide the most useful information. The objectives of the experiment will have the largest bearing on sensor positioning, but the choice of

measurement points may be constrained by accessibility (for example, it might not be possible to mount a sensor under the engine intake).

When attempting to detect low-order vibrations, such as those caused by rotating unbalance and cycle-to-cycle combustion variability, the entire engine tends to vibrate as a unit. In a situation such as this, the measurement location is chosen such that the sensitive axis of the transducer corresponds to the axis of motion that is of interest (Hulls and Welch [18]).

Anderton and Zheng [10] attempted to detect excitations originating in the valve train of an overhead camshaft V6 engine by mounting single-axis accelerometers on the camshaft covers and cylinder head. The rigid physical connection between the camshaft bearings, valve train components, and cylinder head was shown to be a much more efficient path for the transmission of vibrations than the plastic camshaft cover. As a result, the researchers concluded that the cylinder head was more suitable than the camshaft cover as a sensor mounting location when measuring valve train vibrations.

When using accelerometers, the stiffness of the connection between the sensor and the engine will have an effect on the useable frequency range. An example of one extreme is a hand-held probe with an integrated accelerometer. To perform measurements, the probe is pressed by hand against a vibrating surface at various locations of interest. In this case, the useable frequency range would be limited to approximately 1000 Hz due to the extremely low stiffness of the connection between the surface and the sensor [30]. On the other hand, an extremely stiff connection (such as that provided by a strong adhesive or threaded stud mount), would provide useful information up to over 20 kHz [30].

2.3 Techniques for the Diagnosis of Engine Faults

Noise and vibration data generally do not provide much useful information in their raw form - usually it is necessary to apply data processing techniques that extract the relevant information. After the data has been processed, the results must be analyzed and interpreted. The following sections describe some of the techniques that may be used to analyze and interpret engine noise and vibration data.

2.3.1 Time Domain Analysis

Time domain analysis encompasses all techniques that show how a signal fluctuates with respect to time. In general, raw time based data are not very useful for identifying engine malfunctions except for the case where the abnormalities are extreme. Usually, the data are processed using various techniques that help to extract the desired information.

For example, the Root Mean Square (RMS) value of a time-based waveform may be calculated and compared to a threshold value to determine if it is outside acceptable limits. This technique has the advantage that it is simple to implement and the results are simple to interpret. It does not, however, provide any information about the possible source of the abnormality [18].

2.3.2 Crankshaft Angle Domain Analysis

Due to the cyclic nature of engine operation, it is advantageous to synchronize the sampling of data with the rotational speed of the engine. With the aid of a reference

signal, such as the camshaft identification (CID) signal, synchronizing the sampling in this way makes it possible to correlate each acquired data point with a specific point in the engine cycle. This technique is particularly useful for making a connection between an observed abnormality and a specific engine component [17]. Tjong [27] averaged multiple cycles of angle-domain engine data in an attempt to "filter out" random signal components (i.e. noise). It could not be concluded that the noise was completely removed, but the averaging made the repeatable cyclic phenomena much more distinguishable. This is a prime example of an analysis method that is more meaningful when performed in the crankshaft angle domain because the unpredictable variations in the rotational speed of the crankshaft make it difficult to perfectly synchronize time-based sampling with crankshaft motion. Variability in crankshaft speed is caused by cycle-to-cycle and cylinder-to-cylinder variation in combustion pressures.

There are two methods commonly used to acquire angle domain data: synchronous sampling, and synchronous re-sampling. Tjong [27] employed a variance method in which multiple cycles of engine data were collected and processed in the crankshaft angle domain. A ferro-magnetic wheel with 360 teeth was rigidly attached to the engine crankshaft. A magnetic pickup sensed the passage of the teeth on the wheel and generated a signal that was used to trigger data sampling and 'position lock' 720 samples per crank revolution to specific points in the engine cycle. This is an example of synchronous sampling. Chien [11] performed a similar study using the synchronous re-sampling method. Re-sampling refers to a post-processing algorithm in which time-based data is mapped to the angle domain using a signal that tracks the position of the crankshaft.

2.3.3 Frequency Domain Analysis

Many engine phenomena generate vibrations that occur at definite frequencies. For example, the vibrations originating from out-of-balance rotating components are harmonic in nature and may be detected using a narrow band frequency analysis [27]. Other engine malfunctions such as valve impacts, piston slap, excessive bearing clearances, and combustion knock are generally characterized by impulses that contain a particular frequency spectrum. Knowledge of the spectral character associated with engine events makes it possible to identify certain engine faults using narrow band and 1/3 octave procedures [20].

The mathematical basis for frequency analysis is the Fourier Transform. When dealing with digital signals, the Discrete Fourier Transform (DFT) must be used. Cooley and Tukey [55] developed a method for computing the DFT that significantly reduced the number of required computations. The method – known as the Fast Fourier Transform (FFT) – requires that the number of data points be a power of two.

A limitation of Fourier analysis is that it is assumed that the signals being analyzed are perfectly periodic. However, when analyzing "almost periodic" signals such as those obtained from engine vibration measurements, Fourier analysis can provide approximations that are useful in practical situations [12, 13, 15, 19, 20].

2.3.4 Time-Frequency Analysis

Using the Fourier transform to generate one-dimensional frequency spectra is not particularly suitable for transient vibration events that are characterized by time-varying

spectral signatures because the requirement of signal periodicity is violated. A three-dimensional time-frequency representation reveals the temporal localization of a signal's spectral components.

For narrow-band non-stationary signals, the time evolution of the spectral components can be analyzed by performing an FFT on short, successive blocks of data. This technique is known as the Short Time Fourier Transform (STFT). In order to be effective, the successive blocks of data must be short enough to ensure that the spectral character of the signal does not change significantly over the course of the block. For each block, a new spectrum is generated, resulting in a time-frequency representation of the signal. The disadvantage of this technique is that once the frequency resolution is selected, it is fixed throughout the transformation, which means that the high- and low-frequency components are analyzed with the same resolution (Suh [35]). The wavelet transform, a relatively new technique, is similar to the STFT but it has a self-adjusting window size to more efficiently analyze wide-band signals [9, 14, 22, 23].

CHAPTER 3

THEORY

3.1 Internal Combustion Engines

When performing engine vibration studies, it is beneficial to have a sound understanding of internal combustion engines. Knowledge of the relationship between the moving parts within an engine is necessary to properly interpret results. The following sections discuss major engine components and aspects of engine operation that have a profound impact on the nature of engine vibrations. A four-stroke spark ignition (SI) engine was used in this study, so this type of engine will be the focus of these sections. Information pertaining to compression ignition (CI) engines, two-stroke engines, and various other engine types may be found in Stone [32] and Heisler [33].

3.1.1 The Four-Stroke Cycle

The movement of the piston within the engine cylinder from top dead center (TDC) to bottom dead center (BDC), or vice versa, is known as a *stroke*. During each revolution of the crankshaft, there are two strokes of the piston. Therefore, the *four-stroke cycle* is completed in two crankshaft revolutions. The four-stroke cycle can be explained by reference to Figure 3.1.

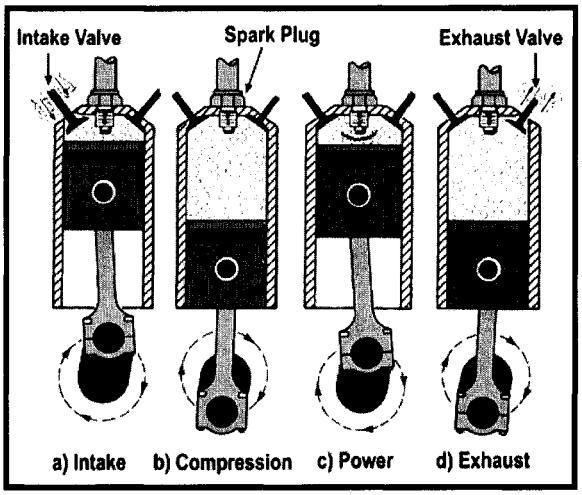

Figure 3.1: The S.I. Engine 4-stroke cycle.

a) The Intake Stroke. The intake valve is open, the exhaust valve is closed, and the piston travels downward drawing fresh air or air/fuel mixture into the cylinder.

b) The Compression Stroke. Both valves are closed, and the piston travels upward compressing the air/fuel mixture. As the piston approaches TDC, the mixture is ignited by the spark plug.

c) The Power Stroke. Both valves are closed. The flame ignited by the spark plug propagates across the combustion chamber causing increases in temperature and pressure. The expanding gases force the piston downward, thus creating power. When the piston is near BDC, the exhaust valve opens and the large difference between the pressure in the cylinder and the pressure in the exhaust manifold causes the exhaust gases in the cylinder to rapidly flow into the exhaust manifold (known as *blow down*).

d) The Exhaust Stroke. The exhaust valve remains open, the intake valve is closed, and the piston travels upward pushing most of the remaining exhaust gases out of the cylinder into the exhaust manifold.

3.1.2 Combustion in Spark Ignition Engines

Combustion can occur either in a normal, controlled manner or in an abnormal manner. The following sections describe what constitutes normal and abnormal combustion in spark ignition engines.

3.1.2.1 Normal Combustion

When the piston approaches top dead center on the compression stroke, a spark is discharged between the spark plug electrodes. The air-fuel mixture in the vicinity of the spark is ignited and forms a small nucleus of flame that begins to propagate into the surrounding unburned mixture. Turbulence in the combustion chamber has the effect of speeding up combustion, but this effect is not observed until the flame nucleus is of the same order of size as the turbulence scale [32]. This fact is partly responsible for what is known as *ignition delay*. The ignition delay period is defined as the time elapsed between the firing of the spark plug and the point at which the in-cylinder pressure history with combustion deviates from the in-cylinder pressure history without combustion (Figure 3.2). The delay period is typically of about 0.5 ms duration [32].

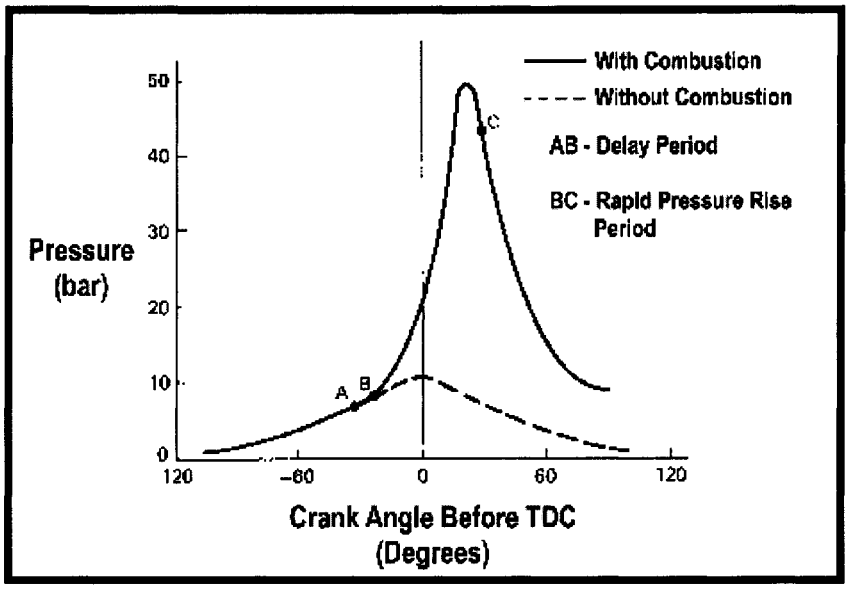

Figure 3.2: Cylinder pressure vs. crank angle with and without combustion.

During the early stages of combustion, when the flame nucleus is small, it can be displaced from the spark plug region by large-scale flows in the cylinder. This generally occurs in a random way, and can have a significant effect on the subsequent propagation of the flame front. These events (known as *cyclic variations*) are manifested by the non-repeatability of successive in-cylinder pressure traces.

After the delay period, there exists a developed flame front that continues to propagate across the combustion chamber until it reaches the cylinder walls. When the energy liberated from the developing flame is sufficient, the cylinder pressure rises at a much faster rate (section B-C in Figure 3.2) until it reaches some peak value, usually at about 5°-20° after top dead center. The time required for the rapid pressure rise depends mainly on the intensity of the in-cylinder turbulence. Turbulence increases almost linearly with engine speed, which in turn causes flame propagation speed to increase [33]. As a result, throughout the engine's speed range the rapid pressure rise phase of

combustion tends to take place over a roughly constant number of degrees of crankshaft rotation.

After the flame front has reached the cylinder walls there will be approximately 25% of the charge which has still not completely burned [33]. At this stage, the burning rate slows down because it becomes more difficult for the remaining oxygen in the charge to react with the vaporized fuel. Heat loss through the cylinder walls, cylinder head, and piston crown and the increasing cylinder volume due to the descending piston cause the pressure in the cylinder to drop rapidly (after point C in Figure 3.2).

3.1.2.2. Abnormal Combustion

Pre-ignition is the ignition of the mixture in the cylinder before the timed spark occurs. It is caused when the mixture comes into contact with a hot surface (or *hot-spot*) such as the exhaust valve, a metal corner in the combustion chamber, or carbon deposits. The propagation of the flame away from the hot-spot is similar to that caused by a spark plug. The difference lies in the instant of ignition - a spark plug provides timed and controlled ignition whereas ignition from hot-spots is rather unpredictable. Pre-ignition leads to higher peak pressures in the cylinder, which can cause self-ignition.

Self-ignition occurs when the pressure and temperature of the unburned air-fuel mixture are such that spontaneous ignition occurs. When the flame propagates away from the spark plug, the resulting expansion of the exhaust gases has the effect of compressing the remaining unburned mixture (or *end gas*). The increase in end gas temperature due to this compression, coupled with the heat radiated from the approaching flame front, can cause the end gas to spontaneously ignite. The resulting pressure waves

pass through the gases in the cylinder at velocities in the range of 1000 m/s – 1200 m/s [33]. These shockwaves reflect against the combustion chamber walls and the walls are set into a state of vibration, producing an audible knocking sound.

3.1.3 Valve Train Dynamics

A schematic of an overhead camshaft layout depicting the main valve train components of the engine used in this study is shown in Figure 3.3.

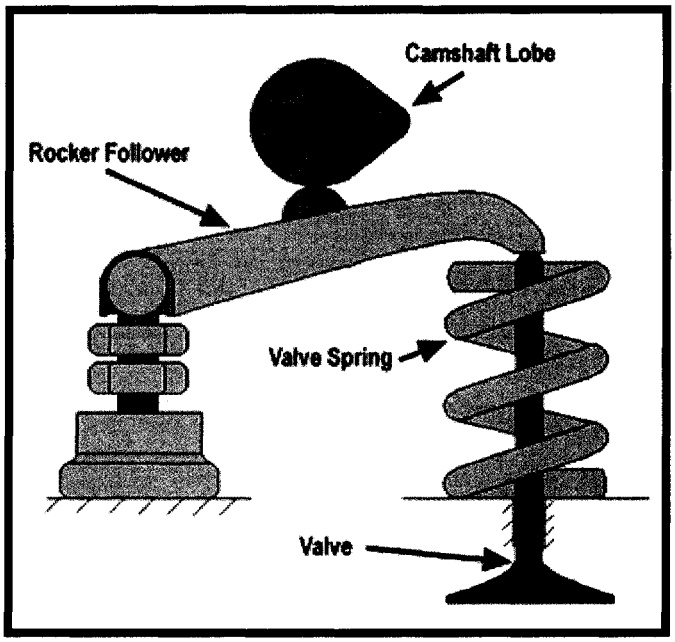

Figure 3.3: Schematic of overhead camshaft valve train.

The valve train system in an automotive engine is designed to meet three primary functional requirements:

1. Maximization of the valve lift area during gas exchange into or out of the combustion chamber during the specified period

2. Reliable operation up to the maximum rated engine speed
3. Minimization of frictional losses

Recently, customer demand for quieter engines has grown, making it necessary for manufacturers to also pay attention to valve train sound quality.

Theoretical valve motion is described by the geometry of the camshaft lobe and its follower. In practice, however, the valve motion will be modified because of the finite mass and stiffness of the elements in the valve train. During the valve-opening period, the rotating cam forces down the valve train components. When this occurs, it is possible for harmonics of the cam profile to excite certain valve train mode shapes [15]. During the valve-closing period, the force applied by the compressed valve spring causes the valve train system to closely follow the cam profile, thus constraining its motion. Valve seating is a typical example of a mechanical impact that generates high frequency vibration in the cylinder head and engine block. Theoretical valve lift, velocity and acceleration are shown in Figure 3.4.

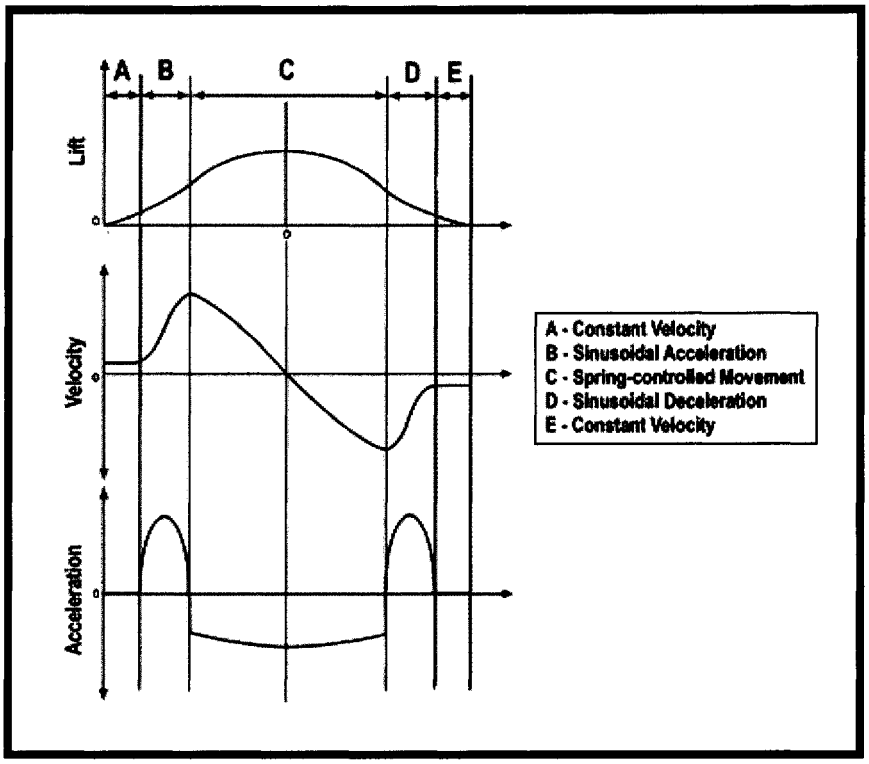

Figure 3.4: Theoretical valve lift, velocity, and acceleration.

For low-speed operation, valve train dynamic effects are not very significant and the valve motion closely follows the cam profile. As the engine speed increases, larger accelerations and forces are imposed on the system immediately following the start of valve opening, and just before valve closing (Figure 3.5). For this reason, proper valve train design is particularly important when high engine speeds are considered [33].

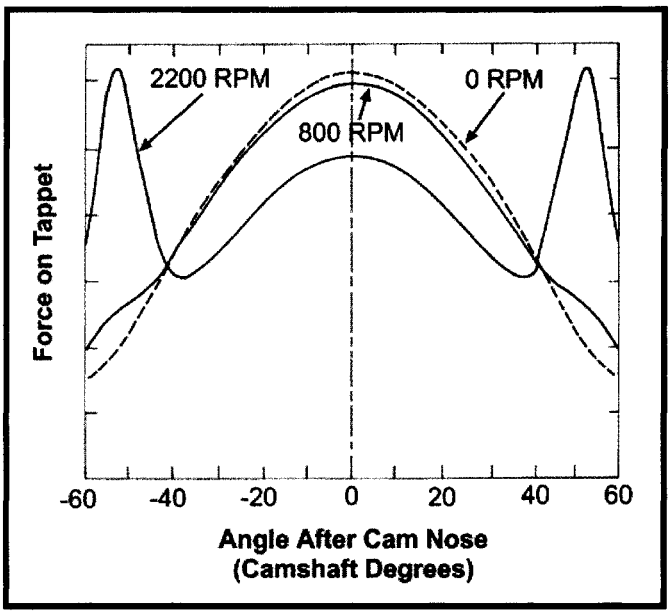

Figure 3.5: Variation with RPM of force on tappet.

3.2 Vibration

Vibration is the oscillatory motion of an object or surface relative to a stationary frame of reference. In order for a system to vibrate, it must have a component that is capable of storing potential energy and releasing it in the form of kinetic energy of a mass. This kinetic energy is then given up to the potential energy of the storing device and the cycle repeats itself. The fundamental kinematical properties that are used to describe the motion of a particle are the vectors of displacement, velocity, and acceleration. For the case of rectilinear motion, the vectors reduce to scalars and these properties are related to each other as follows:

$$v(t) = \frac{dx(t)}{dt} = \dot{x}(t)$$
$$a(t) = \frac{dv(t)}{dt} = \frac{d^2x(t)}{dt^2} = \ddot{x}(t) \qquad (3\text{-}1)$$

Where: $x(t)$ = linear displacement with respect to time
$v(t)$ = linear velocity with respect to time
$a(t)$ = linear acceleration with respect to time

For the more general case where motion is not rectilinear, equations 3-1 may be applied separately to three independent directions.

A single degree-of-freedom spring-mass-damper system, and the corresponding free body diagram, are shown in Figure 3.6.

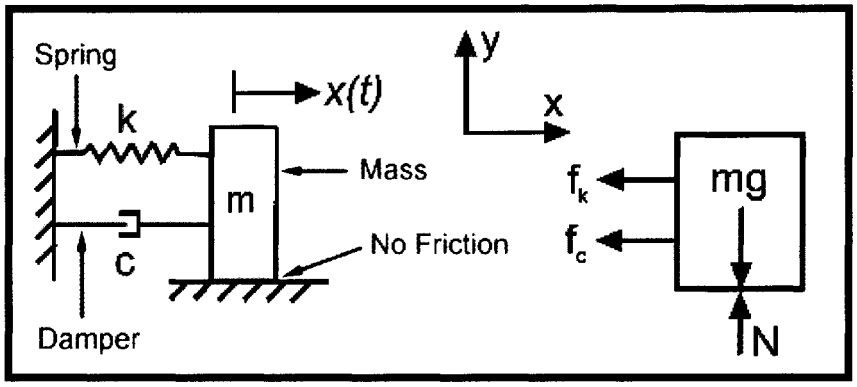

Figure 3.6: Schematic and free body diagram of a single degree-of-freedom system.

The spring in Figure 3.6 is a model for storing kinetic energy, and is characterized by its stiffness *k*. The damper in the figure is a model for dissipation of energy, and is characterized by its damping coefficient *c*. As shown in the free body diagram, the spring and damper exert forces on the mass. These forces are calculated as follows:

$$f_k = -kx(t) \qquad \text{(3-2a)}$$

$$f_c = -c\dot{x}(t) \qquad \text{(3-2b)}$$

The negative signs represent the fact that the forces act so as to *oppose* motion, and the dot in equation 3-2b denotes a single differentiation with respect to time. Equation 3-2a

is a form of *Hooke's Law* which states that the restoring force exerted by a spring is directly proportional to the deformation of the spring (in this case, the deformation of the spring is equal to the displacement of the mass). The inherent assumption in equation 3.2b is that the damping force is proportional to the velocity of the mass. This concept is generally accepted, and has been shown to provide reasonably accurate approximations of physical systems [26]. With proper understanding, variations of the spring-mass-damper system can be used to model the vibration of virtually any mechanical system.

A simple force balance on the mass m shown in Figure 3.6 may be performed as follows:

$$-f_c - f_k = ma(t)$$

Where: f_c = force exerted on mass by damper
f_k = force exerted on mass by spring

Substituting in equations 3-1 and 3-2 and rearranging gives:

$$m\ddot{x}(t) + c\dot{x}(t) + kx(t) = 0 \qquad (3\text{-}3)$$

Equation 3-3 is the general *equation of motion* for a damped single-degree-of-freedom system. If the special case of Equation 3-3 where c is equal to zero is considered (i.e. the system is *undamped*), the equation of motion becomes:

$$m\ddot{x}(t) + kx(t) = 0 \qquad (3\text{-}4)$$

To solve equation 3-4, let us assume that the solution takes the following form:

$$x(t) = A\sin(\omega t + \phi) \qquad (3\text{-}5)$$

Substitution of equation 3-5 into equation 3-4 yields:

$$-m\omega^2 A\sin(\omega t + \phi) = -kA\sin(\omega t + \phi) \qquad (3\text{-}6)$$

In order to satisfy equation 3-6, it is required that:

$$\omega = \sqrt{\frac{k}{m}} \tag{3-7}$$

The quantity ω in equation 3-7 is known as the *undamped natural frequency* of the system. In order to determine the correct values for the parameters A and ϕ in Equation 3-5, two initial conditions are required:

$$x(0) = x_0 \tag{3-8}$$
$$\dot{x}(0) = v(0) = v_0$$

Where: x_0 = initial value of displacement
v_0 = initial value of velocity

Substituting the values for the initial conditions into the equations for displacement and velocity and solving the equations simultaneously yields the following results:

$$A = \frac{\sqrt{\omega^2 x_0^2 + v_0^2}}{\omega} \tag{3-9a}$$

$$\phi = \tan^{-1}\frac{\omega x_0}{v_0} \tag{3-9b}$$

Finally, substitution of equations 3-7, 3-9a, and 3-9b into Equation 3-5 yields the solution of the equation of motion, or *displacement response*, for the spring-mass system:

$$x(t) = \frac{\sqrt{\omega^2 x_0^2 + v_0^2}}{\omega}\sin\left(\omega t + \tan^{-1}\frac{\omega x_0}{v_0}\right) \tag{3-10}$$

This solution is known as the *free response* because no force external to the system is applied after $t = 0$.

If damping is included in the analysis, the solution must be obtained by solving Equation 3-3 for the case where c assumes a positive non-zero value. The solution of this

equation is well established in the theory of elementary differential equations. First, it is assumed that the solution *x(t)* is of the following form:

$$x(t) = ae^{\lambda t} \tag{3-11}$$

Where: a and λ are constants to be determined

Differentiating Equation 3-11 twice, the following expressions for velocity and acceleration are obtained:

$$\dot{x}(t) = \lambda a e^{\lambda t} \tag{3-12a}$$

$$\ddot{x}(t) = \lambda^2 a e^{\lambda t} \tag{3-12b}$$

Substituting equations 3-11 and 3-12 into Equation 3-3 results in the following:

$$m\lambda^2 a e^{\lambda t} + c\lambda a e^{\lambda t} + k a e^{\lambda t} = 0 \tag{3-13}$$

Since the term $ae^{\lambda t}$ is never zero, it may be divided out of Equation 3-13 to give the so-called *characteristic equation*:

$$m\lambda^2 + c\lambda + k = 0 \tag{3-14}$$

Applying the quadratic formula to Equation 3-14 yields the following solutions:

$$\lambda_{1,2} = \frac{-c \pm \sqrt{c^2 - 4km}}{2m} \tag{3-15}$$

The general characteristics of the system response are determined by whether the discriminant c^2-$4km$ in Equation 3-15 turns out to be positive, negative, or zero. For this reason, it is convenient to define a *critical damping coefficient* which causes the discriminant to equal zero:

$$c_{cr} = 2\sqrt{km} = 2m\omega \tag{3-16}$$

Another convenient parameter is the non-dimensional *damping ratio* defined as follows:

$$\zeta = \frac{c}{c_{cr}} = \frac{c}{2m\omega} \tag{3-17}$$

If Equations 3-16 and 3-17 are substituted into Equation 3-15, the roots of the characteristic equation may be expressed as:

$$\lambda_{1,2} = -\zeta\omega \pm \omega\sqrt{\zeta^2 - 1} \tag{3-18}$$

The spring-mass-damper system may now be classified as one of the following:

1. *underdamped* ($0 < \zeta < 1$)
2. *critically damped* ($\zeta = 1$)
3. *overdamped* ($\zeta > 1$)

Each of these cases will be described in the following sections.

1. Underdamped Motion ($0 < \zeta < 1$)

In this case, the damping ratio ζ is less than unity, and the discriminant in Equation 3-18 is negative, resulting in a complex conjugate pair of roots:

$$\lambda_1 = -\zeta\omega - \omega\sqrt{1-\zeta^2}\,j \tag{3-19a}$$

$$\lambda_2 = -\zeta\omega + \omega\sqrt{1-\zeta^2}\,j \tag{3-19b}$$

Where: $j = \sqrt{-1}$

Due to linearity, the sum of the two solutions is also a solution. Thus, the displacement response for the case of underdamped motion takes the following form:

$$x(t) = e^{-\zeta\omega t}\left(a_1 e^{j\sqrt{1-\zeta^2}\omega t} + a_2 e^{-j\sqrt{1-\zeta^2}\omega t}\right) \tag{3-20}$$

Where a_1 and a_2 are constants of integration to be determined by the initial conditions. Applying the Euler identity, Equation 3-20 can be expressed as:

$$x(t) = Ae^{-\zeta\omega t}\sin(\omega_d t + \phi) \tag{3-21}$$

Where: $\omega_d = \omega\sqrt{1-\zeta^2}$

A = constant of integration, determined by initial conditions

ϕ = constant of integration, determined by initial conditions

The quantity ω_d in Equation 3-21 is known as the *damped natural frequency* of the system, and it is the frequency at which the system will freely vibrate when damping is present.

Applying x_0 and v_0, the initial conditions for displacement and velocity respectively, the constants of integration in Equation 3-21 become:

$$A = \sqrt{\frac{(v_0 + \zeta\omega x_0)^2 + (x_0\omega_d)^2}{\omega_d^2}} \tag{3-22a}$$

$$\phi = \tan^{-1}\left(\frac{x_0\omega_d}{v_0 + \zeta\omega x_0}\right) \tag{3-22b}$$

In general, it can be stated that an underdamped system oscillates with decaying amplitude. The rate of decay is determined by the damping ratio ζ. An example of an underdamped response is shown in Figure 3.7. This type of response is by far the most common in practical mechanical systems.

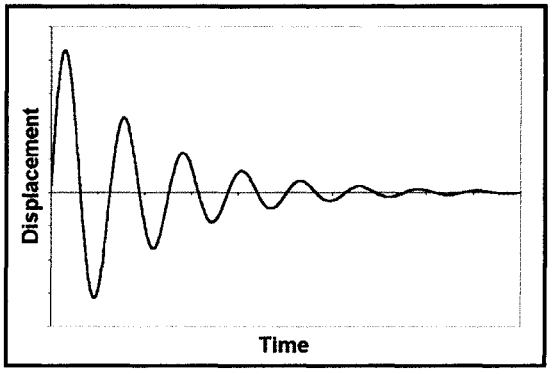

Figure 3.7: Example of underdamped response ($\zeta < 1$).

2. Critically Damped Motion ($\zeta = 1$)

For this case, the damping ratio ζ is unity and the discriminant in Equation 3-18 is identically equal to zero. This threshold value of ζ represents the separation point between oscillatory motion and non-oscillatory motion. With the discriminant equal to zero, the following repeated roots are obtained:

$$\lambda_1 = \lambda_2 = -\omega \tag{3-23}$$

From elementary differential equations, it is known that the solution takes the form:

$$x(t) = (a_1 + a_2 t)e^{-\omega t} \tag{3-24}$$

Again, a_1 and a_2 are constants of integration that are determined through application of the initial displacement and velocity:

$$a_1 = x_0 \tag{3-25a}$$
$$a_2 = v_0 + \omega x_0 \tag{3-25b}$$

Examples of critically damped motion are shown in Figure 3.8 for two different sets of initial conditions.

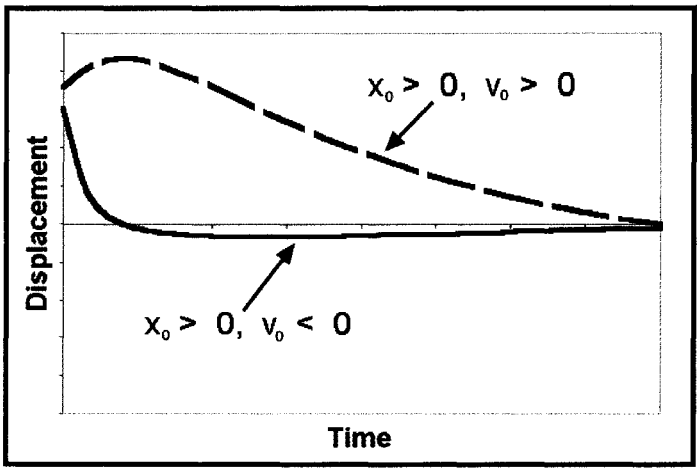

Figure 3.8: Examples of critically damped motion (ζ=1).

3. Overdamped Motion ($\zeta > 1$)

In this case, the damping ratio ζ is greater than unity, and the discriminant in Equation 3-18 is positive. This results in a pair of distinct real roots that are expressed as follows:

$$\lambda_1 = -\zeta\omega - \omega\sqrt{\zeta^2 - 1} \tag{3-26a}$$

$$\lambda_2 = -\zeta\omega + \omega\sqrt{\zeta^2 - 1} \tag{3-26b}$$

Thus, the equation of motion for an overdamped system becomes:

$$x(t) = e^{-\zeta\omega t}(a_1 e^{-\omega\sqrt{\zeta^2-1}t} + a_2 e^{\omega\sqrt{\zeta^2-1}t}) \tag{3-27}$$

The constants a_1 and a_2 are determined through application of the initial conditions:

$$a_1 = \frac{-v_0 + (-\zeta + \sqrt{\zeta^2 - 1})\omega x_0}{2\omega\sqrt{\zeta^2 - 1}} \tag{3-28a}$$

$$a_2 = \frac{v_0 + (\zeta + \sqrt{\zeta^2 - 1})\omega x_0}{2\omega\sqrt{\zeta^2 - 1}} \tag{3-28b}$$

Upon inspection of Equation 3-27, it can be seen that an overdamped response is non-oscillatory, and it returns to its rest position exponentially. Examples of overdamped motion are shown in Figure 3.9.

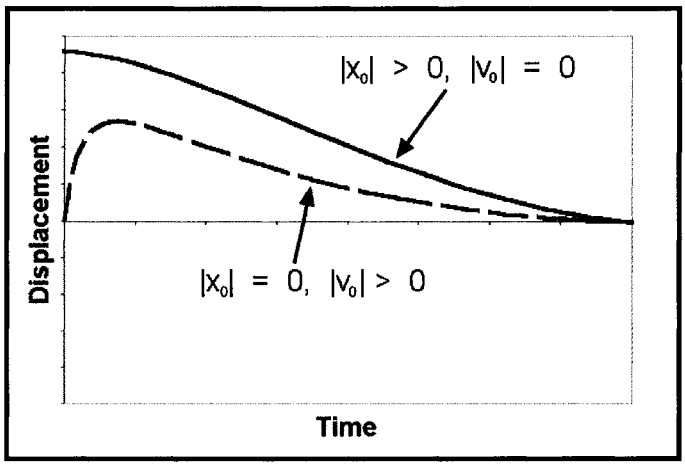

Figure 3.9: Examples of overdamped motion (ζ>1).

3.3 Engine Dynamometers

It is important to have the ability to control the speed and load conditions of the engine when performing NVH studies. This control is often provided by means of an *engine dynamometer*. A schematic of a typical dynamometer setup is shown in Figure 3.10.

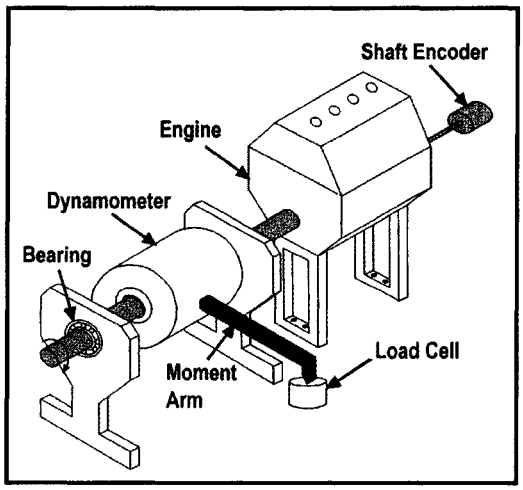

Figure 3.10: Schematic of a typical engine dynamometer setup.

The main purpose of an engine dynamometer is to resist the rotation of the engine crankshaft. In steady state testing, the use of a dynamometer permits engine tests to be carried out in one of three modes: constant engine speed, constant torque, and constant throttle opening. To illustrate the concept of an engine dynamometer, a simple mechanical brake is shown in Figure 3.11.

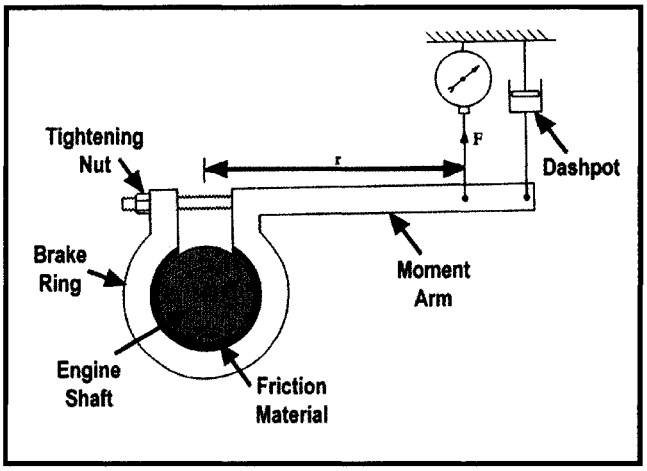

Figure 3.11: Mechanical brake showing principles of dynamometer operation.

The rotation of the engine shaft is resisted by the brake ring due to friction. The amount of resistance can be adjusted by the nut shown in the figure. The brake ring is stopped from rotating by the moment arm. The force required to stop moment arm rotation is measured by means of a simple scale. The purpose of the dashpot damper is to damp out oscillations caused by the fluctuating torque output of the engine.

Referring to Figure 3.11, the torque that the engine must develop in order to overcome the brake resistance can be calculated as follows:

$$T = Fr \tag{3-29}$$

Where: T = torque
r = length of moment arm

F = force required to stop moment arm rotation

The power developed by the engine and absorbed by the brake can be calculated from the following equation:

$$P = T\omega \tag{3-30}$$

Where: P = power (watts)

$\omega = \frac{2\pi N}{60}$ = angular velocity of shaft (rad/s)

N = engine rotational speed (RPM)

Dynamometers that rely on friction to resist the rotation of the engine crankshaft and spring scales to measure force have become obsolete. Most modern dynamometers employ electromagnetic fields to resist rotation and transducers known as load cells to measure the force acting on the moment arm. Transducers that measure torque directly without the need of a moment arm are also available, but they are considerably more expensive.

3.3.1 Electrical Dynamometers

In electrical dynamometers, the shaft rotation drives an electrical generator. The strength of the electromagnetic field coupling the rotating and stationary parts of the dynamometer can be adjusted in order to increase or decrease the resistance offered to engine rotation. A great advantage of this concept is that the strength of the electromagnetic field can be altered almost instantly, providing fast and easy control over the amount of resistance applied to engine rotation.

With electrical dynamometers, the engine power is converted to electrical energy which can be transferred away from the dynamometer by cables or dissipated as heat.

There are three main types of electrical dynamometer: direct current (DC), alternating current (AC) and eddy current.

DC and AC dynamometers utilize DC and AC generators, respectively. The function of these generators may be reversed so that they act as electric motors. This characteristic is useful because it makes it possible to "motor" the engine without combustion. Measuring engine noise and vibration without combustion is desirable in some cases because combustion is a major source of noise that may mask the phenomena of interest. AC and DC dynamometers are capable of very rapid changes in the resisting torque offered to the engine, and are well-suited for microprocessor control. However, they are not capable of rapid speed changes because their rotating parts have high inertia.

Eddy current dynamometers are very common in research laboratories. In this type of dynamometer, the electrical power generated is dissipated within the dynamometer itself, and the energy is carried away by cooling water. Eddy current systems are of relatively simple and robust design, but they do not offer the ability to act as an electric motor. Eddy current dynamometers are readily controllable by a microprocessor, and their resisting torque can be altered almost instantly. As well, their ability to change speeds is superior to that of an AC or DC machine due to lower rotor inertia.

3.4 Data Acquisition

When dealing with sampled time signals, and their subsequent transformation to the frequency domain, there are many concepts that must be understood in order to ensure

the accuracy and validity of the results. In the sections that follow, many of these important concepts are discussed.

3.4.1 Sampling Theory

An *analog signal* is a continuously varying voltage. Transducers that are used to measure physical phenomena usually output analog signals that are proportional to the physical variable being measured. These analog signals are sampled and converted to discrete digital information by means of a process known as *analog to digital conversion* or *quantization.* Sampling can be thought of as a process where the continuous analog signal is multiplied by a unity amplitude discrete-valued sampling function. The result is a discrete time history (i.e. amplitude values are equally spaced in time).

The spacing between values in the sampled signal is related to the sampling rate as follows:

$$F_s = \frac{1}{\Delta t} \tag{3-31}$$

Where: F_s = sampling rate or sampling frequency
Δt = time spacing of samples

In order to extract valid frequency information, care must be taken in choosing an appropriate sampling rate. *Shannon's Sampling Theorem* states that the sampling rate should be at least twice the highest frequency of interest in the measurement signal [4]:

$$F_s > 2f_{max} \tag{3-32}$$

Where: f_{max} = maximum frequency of interest
$\frac{F_s}{2}$ = so-called *Nyquist* frequency

If accurate information is required at f_{max}, the literature suggests that it is good practice to sample at a minimum of 2.56 times this frequency because information at exactly the Nyquist frequency is generally not very reliable [1, 2, 4]. Figure 3.12 illustrates how well a pure tone signal (i.e. a sine wave) is reproduced in the time domain with different sampling frequencies.

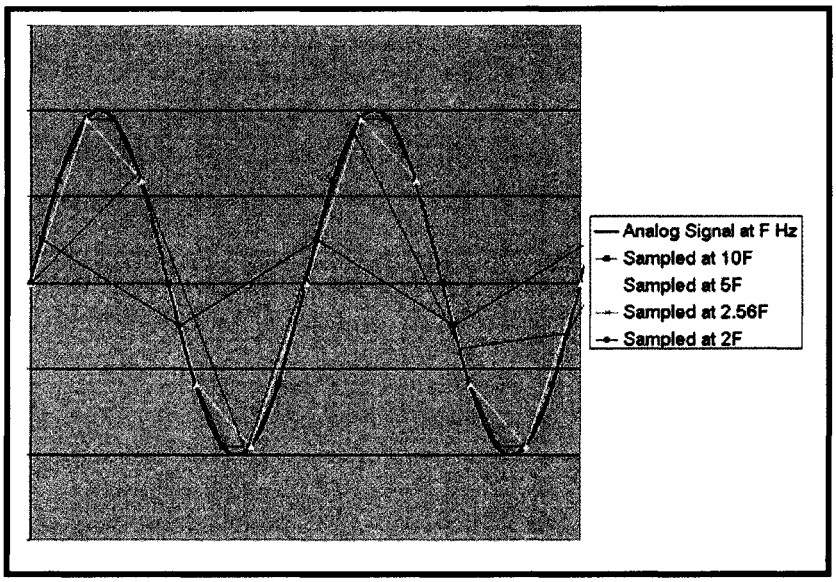

Figure 3.12: Reproduction of sine wave with different sampling rates.

The lowest resolvable frequency, or the *frequency resolution*, is determined by the length of the measurement period:

$$\Delta f = \frac{1}{T} \qquad (3\text{-}33)$$

Where: Δf = frequency resolution
T = length of measurement or measurement period

Equation 3-33 is intuitively obvious because it states that in order to resolve a given frequency, the measurement period must be long enough to capture at least one full cycle at that frequency.

3.4.2 Aliasing

Signal components that occur at a frequency greater than f_{max} in the analog time history will cause amplitude and frequency errors in the computed frequency spectrum. This error is known as *aliasing*. A simple illustration of aliasing is shown in Figure 3.13.

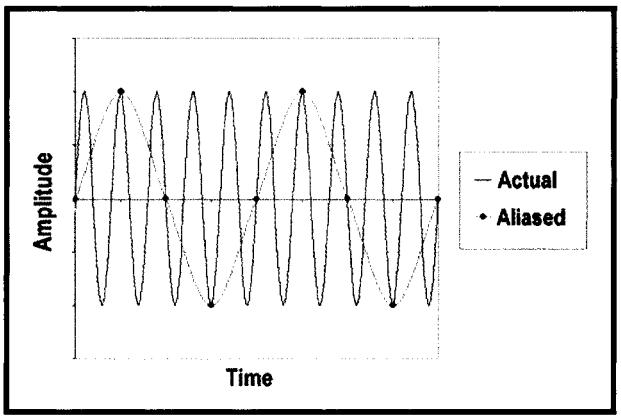

Figure 3.13: Example of aliasing in the time domain.

The red dots in the figure represent the points at which samples of the actual analog signal are acquired. The red line running through the dots is the curve that is inferred from the sampled data. Although the waveform generated from the sampled data is sinusoidal in nature, it clearly suggests a frequency much lower than that of the actual analog signal. This error is due to the fact that the analog signal is being sampled at a rate less than twice its frequency, and thus the conditions of Shannon's Sampling Theorem (Equation 3-32) are not being met. A frequency that occurs above f_{max} in the analog time history will "fold back" and appear below f_{max} in the computed spectrum. This concept is illustrated in Figure 3.14.

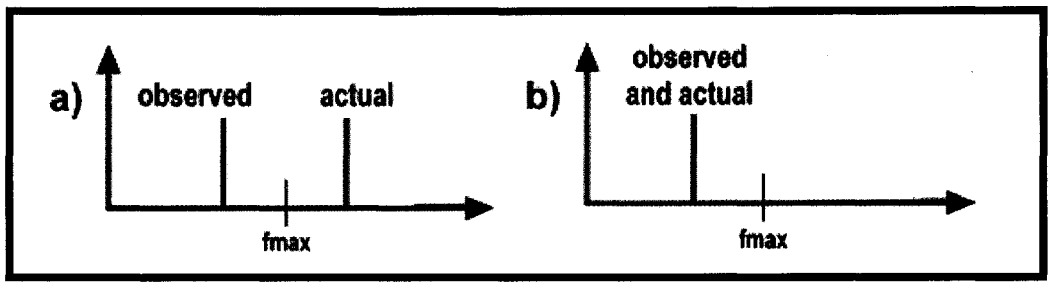

Figure 3.14: a) Frequency fold back (aliasing); b) No aliasing (proper selection of sample rate).

In many practical situations it is impossible to know what will be the maximum frequency contained in an analog signal that is to be measured. Even if the maximum frequency is known, the available data acquisition hardware might not be capable of sampling fast enough to prevent aliasing. To address this problem, most modern data acquisition systems employ an *anti-aliasing filter*. An anti-aliasing filter is essentially an analog low-pass filter that attenuates any portion of the analog time history that lies above half of the chosen sampling frequency. Since the analog signal is filtered before it is digitized, aliasing is avoided. It is vital that the low-pass filter be applied to the analog signal *before* sampling because after a signal is digitized it is impossible to distinguish between legitimate components and aliased components.

3.4.3 Quantization

An Analog-to-Digital Converter (ADC) is a hardware device comprised of circuitry capable of sampling an analog signal and converting it to digital information that may be stored, displayed, or analyzed in real time. An ADC can be integrated into a circuit board that may be installed in an expansion slot of a desktop computer or external

front-end chassis. Digital oscilloscopes are standalone units with built-in ADC's and monitors for displaying the digitized information.

As mentioned previously, an ADC converts and analog voltage into a binary number through a process called quantization. The process takes place one sample at a time. For the analog input signals, the usable voltage range is specified in terms of the *full-scale voltage range*. Typical ranges are 0 to 10 V (unipolar) or –5 to 5 V (bipolar). Voltages outside of this range will not be digitized properly and, in extreme cases, may damage the circuitry. The digital side of the ADC is specified in terms of the number of bits in its register. The number of bits dictates how many discrete levels are resolvable over the full-scale voltage range. For example, a 12-bit ADC divides the full-scale voltage range into $2^{12} = 4096$ levels. The smallest reproducible analog signal is thus determined as follows:

$$\Delta A_{sig} = \frac{FS}{2^N} \tag{3-34}$$

Where: ΔA_{sig} = smallest resolvable change in signal amplitude
FS = full-scale voltage range
N = number of bits in the ADC register

3.5 Data Analysis Methods

The manner in which data are analyzed will determine what information is ultimately obtained. The capabilities of modern computers make it possible to apply mathematically intensive analysis techniques in relatively short periods of time. In the following sections, some of the techniques that are applicable to engine vibration studies will be discussed.

3.5.1 Time Domain Analysis

Time domain analysis embodies all techniques that deal with measurement signals that are represented as a function of time. In general, raw time-based data are difficult to interpret. Usually, the data must be processed in some way before any useful information can be extracted.

3.5.1.1 Raw Data Comparison

Two vibration signals that were taken from the cylinder block of a V8 engine are shown in Figure 3.15.

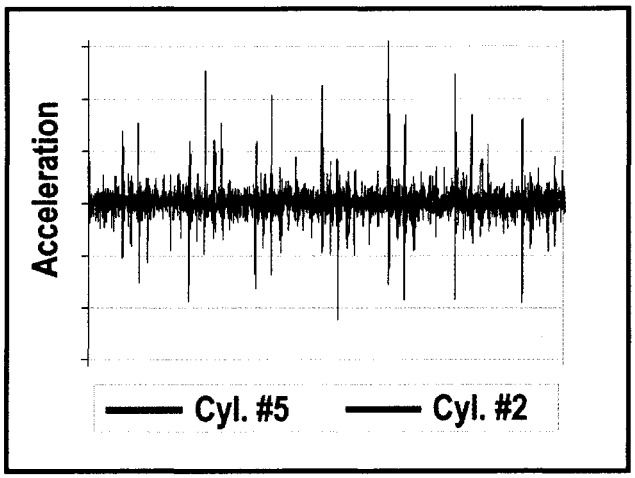

Figure 3.15: Vibration signals measured from two locations on engine block.

This particular engine had a severe 'cold knock' in cylinder #5. *Cold knock* is a type of piston slap caused by excessive piston-to-bore clearance when the engine is cold. Usually, the noise generated by this type of problem dissipates as the engine warms up because the excessive clearance is reduced by thermal expansion of the piston. It can be seen in the figure that the data taken from cylinder #5 contains large-amplitude

acceleration spikes that correspond to the piston slap events. In contrast, the data taken from cylinder #2 contains no abnormally large acceleration spikes. The spikes that are visible in the cylinder #2 data are due to normal combustion, and are to be expected.

This simple type of analysis has the advantage that it requires no data processing and it may be performed quickly and easily. However, the only conclusion that can be reached using this method is that the knocking noise is originating in the vicinity of cylinder #5. Since there is no engine cycle reference available, there is no way of determining where in the cycle the noise is occurring, or how many times per cycle the noise is occurring. If this information is required, crankshaft angle domain analysis is far more appropriate.

3.5.1.2 Root-Mean-Square (RMS) Analysis

The root-mean-square (RMS) value of a measurement signal may be used in some situations to locate an engine defect. RMS is calculated as follows:

$$X_{RMS} = \sqrt{\frac{1}{N}\sum_{i=1}^{i=N} x_i^2} \tag{3-35}$$

Where: X_{RMS} = signal RMS value
x_i = ith data sample
N = number of data samples

RMS provides a very useful single-parameter measure of the energy content of a diagnostic signal. Figure 3.16 shows the RMS amplitudes of acceleration signals acquired from each cylinder of a noisy V6 engine operating at idle (~750 RPM).

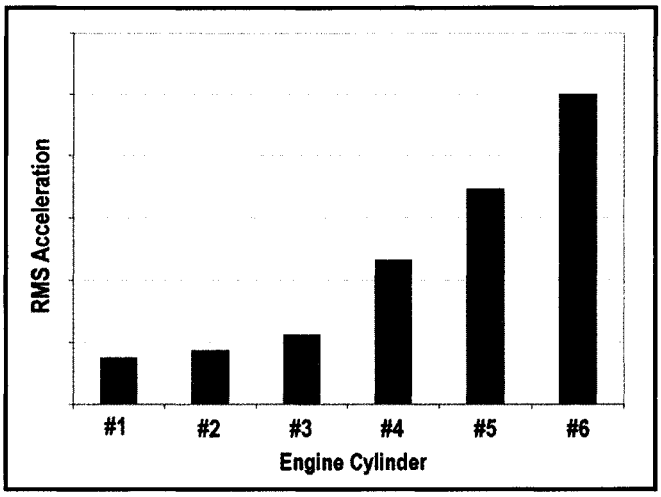

Figure 3.16: RMS acceleration values for each cylinder of a V6 Engine.

This particular engine had four circular grooves on the liner of cylinder bore #6. The piston rings traversing the grooves caused the surface of the engine block near cylinder #6 to vibrate at amplitudes much larger than those observed at the other cylinders. The abnormal vibration is manifested in Figure 3.16 in the cylinder #6 RMS value. The accelerometers mounted on cylinders #4 and #5 were also able to detect the vibration excited in cylinder #6 because cylinders #4, #5, and #6 belong to the same cylinder bank.

RMS analysis has the advantage that it is easy to implement and the results are easy to interpret. However, since it is solely a measure of signal energy content, it provides no information about signal characteristics that might assist the analyst in locating a specific defect.

3.5.1.3. Linear Averaging

If a periodic signal is hidden by noise, in some cases the noise may be removed or reduced using the technique of *linear averaging*. Linear averaging can be implemented if

a trigger signal that is synchronous with the periodic part of the measurement signal is available. The synchronizing signal is used to trigger the start of a time record. If properly implemented, the periodic part of the input will be the same in each acquired time record, whereas the noise will vary randomly. The linear average is obtained by adding together each of the time records and dividing the sum by the number of time records:

$$\bar{y}(t_i) = \frac{1}{N}\sum_{k=1}^{N} y_k(t_i) \tag{3-36}$$

Where: $\bar{y}(t_i)$ = linear average of signal $y(t)$ at i^{th} point in time record
N = number of time records acquired

Since the periodic signal will repeat itself in each time record, it will average to some finite value. If the noise component is comprised of pure Gaussian noise (i.e. *white* noise), then it will average out to zero. In most practical situations, the noise will not have a perfect Gaussian distribution, but nonetheless, averaging has the effect of greatly improving the signal-to-noise ratio [4]. To illustrate, Figure 3.17 shows a single time record compared with a linear average of 40 time records.

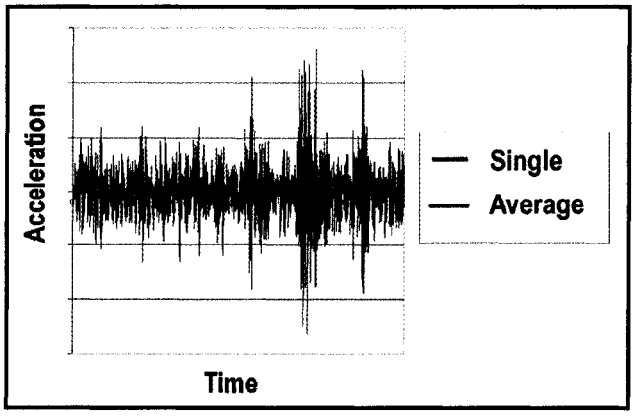

Figure 3.17: Single data record and average of 40 records.

Due to cycle-to-cycle and cylinder-to-cylinder variations in combustion pressures, it is impossible to keep an engine's operating speed perfectly constant. For this reason, the number of data points acquired between each of the trigger pulses is constantly varying. Linear averaging is much more suitable for the crankshaft angle domain, where data can be decomposed into discrete engine cycles comprised of the same number of data points.

3.5.2 Frequency Domain Analysis

Frequency analysis is used to decompose a complex signal into its components at various frequencies. Engine measurement signals observed in the frequency domain can reveal characteristics that are impossible to distinguish in the crankshaft angle domain or time domain.

3.5.2.1 Complex Notation

Frequency components may be thought of as rotating vectors (or *phasors*) that are represented mathematically as complex exponentials. Figure 3.18 depicts a two-dimensional vector F in the so-called *complex plane*.

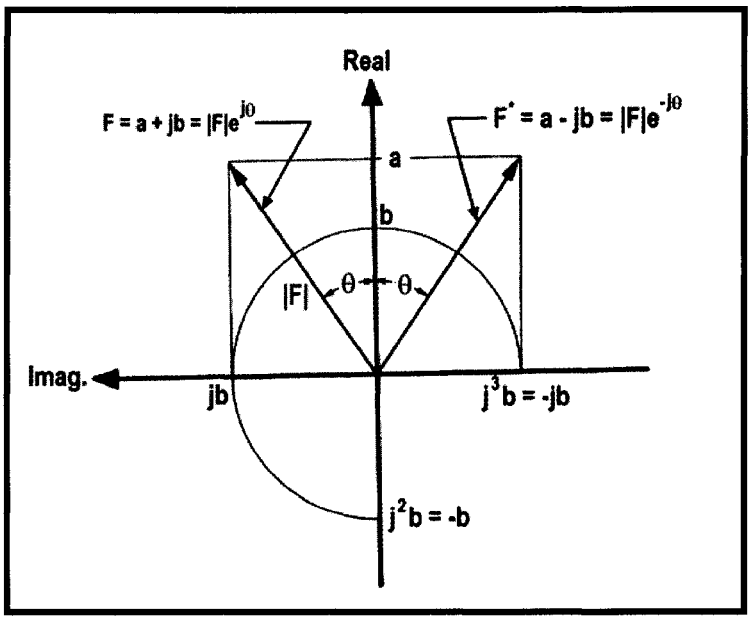

Figure 3.18: Complex plane representation of a frequency component.

The vector is the sum of a real component a directed along the real axis and an imaginary component jb directed along the imaginary axis:

$$F = a + jb \qquad (3\text{-}37a)$$

where: $j = \sqrt{-1}$

If the sign of the complex component is reversed, the result is the so-called *complex conjugate*. The complex conjugate is usually denoted by an asterisk superscript as follows:

$$F^* = a - jb \qquad (3\text{-}38b)$$

The complex conjugate is important when calculating various frequency domain functions that will be discussed later in this chapter.

3.5.2.2 Fourier Analysis

The mathematical basis of frequency analysis is the Fourier Transform, which takes different forms depending on the type of signal being analyzed. The common thread among them all is that the signal is always assumed to be composed of a number (possibly an infinite number) of sinusoidal components at various frequencies, each having a given amplitude and initial phase. A simple sinusoidal component, represented two different ways, is shown in Figure 3.19.

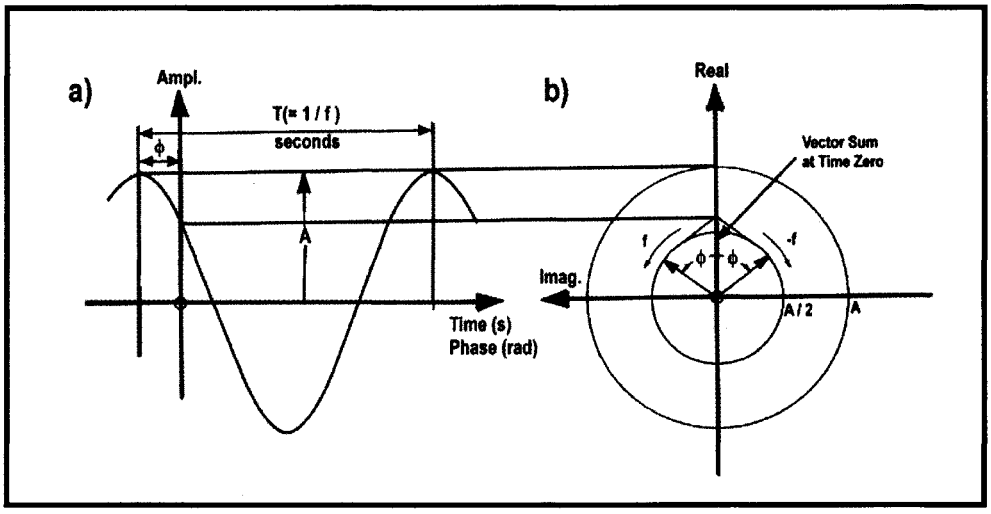

Figure 3.19: Two different representations of a (co-) sinusoidal component.

The representation in the left of the figure has the distinction that both time and phase are represented on the horizontal axis. The representation on the right shows the same sinusoidal component as the vector sum of two contra-rotating vectors, each with amplitude *A/2*. One has initial phase angle ϕ and rotates with frequency *f* while the other has initial phase $-\phi$ and rotates with frequency *–f*. The concept of negative frequency has the physical interpretation of indicating a negative rate of change of phase angle. It can

be seen that as the two vectors rotate with time, the vector sum will always be real because the imaginary parts cancel out.

The equivalence of the two representations is due to the following identity [4]:

$$A\cos\theta = \frac{A}{2}\left(e^{j\theta} + e^{-j\theta}\right) \tag{3-39}$$

Where: $\theta = 2\pi ft + \phi$
f = frequency in Hertz
t = time in seconds
ϕ = initial phase

The following is the general form of a periodic function:

$$y(t) = y(t + nT) \tag{3-40}$$

Where: T = period of signal
n = any integer

Any periodic function may be represented as a sum of sinusoidal components (or, equivalently, rotating vectors) at equally spaced frequencies kf_1 where f_1 is the reciprocal of the periodic time T, and k is any integer. The k^{th} component is obtained from the following integral:

$$Y(f_k) = \frac{1}{T}\int_{\frac{-T}{2}}^{\frac{T}{2}} y(t)e^{-j2\pi f_k t}\,dt \tag{3-41}$$

Equation 3-41 has the effect of *extracting* from $y(t)$ the components it contains at each frequency f_k. The value of the original function may be calculated at any instant in time as the vector sum of all vectors in their instantaneous positions:

$$y(t) = \sum_{-\infty}^{\infty} Y(f_k)e^{j2\pi f_k t} \tag{3-42}$$

The series of complex values $Y(f_k)$ are known as the spectral components of $y(t)$. Since there are real and imaginary parts associated with each one, a full visual representation requires three dimensions (Figure 3.20).

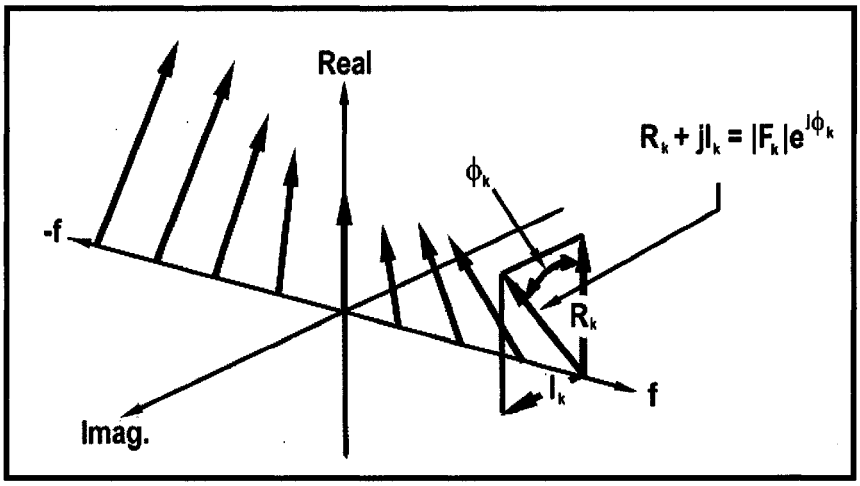

Figure 3.20: Three-dimensional representation of a frequency spectrum.

It is possible to extend Equation 3-41 to a more general case by letting the periodic time T approach infinity, in which case the spacing $1/T$ between the spectral components tends to zero and $Y(f)$ becomes a continuous function of frequency:

$$Y(f) = \int_{-\infty}^{\infty} y(t)e^{-j2\pi ft}\,dt \tag{3-43}$$

In this case, Equation 3-42 becomes:

$$y(t) = \int_{-\infty}^{\infty} Y(f)e^{j2\pi ft}\,df \tag{3-44}$$

Equation 3-43 is known as the *Forward Fourier Transform* and Equation 3-44 is known as the *Inverse Fourier Transform.*

There is yet another form of the Fourier Transform that applies to functions that are represented by a sequence of values sampled at discrete, equally-spaced points in

time. This case is becoming very important due to the modern widespread use of digital processing techniques. The so-called *Discrete Fourier Transform* (DFT) takes the following form:

$$Y(k) = \frac{1}{N}\sum_{n=0}^{N-1} y(t_n) e^{\frac{-j2\pi f_k t_n}{N}} \tag{3-45}$$

The inverse of this is the following:

$$y(t_n) = \sum_{k=0}^{N-1} Y(f_k) e^{\frac{j2\pi f_k t_n}{N}} \tag{3-46}$$

In order to obtain N frequency components from N time samples (or vice versa), N^2 complex multiplications must be performed [4]. A calculation procedure known as the *Fast Fourier Transform* (FFT) provides the same results as the DFT, but it requires a number of complex multiplications on the order of $N\log_2(N)$, which is significantly less than the number of computations required for the DFT [55]. In order to perform the FFT, however, the number of points in the data record must be a power of two.

When the Fourier transform is applied to a time history, the result is known as a *linear spectrum*. However, there are other ways of presenting data in the frequency domain. Some of the standard frequency functions are discussed in the following sections.

3.5.2.3 Autopower Spectrum

The *autopower spectrum* is a function defined as the linear spectrum multiplied by its complex conjugate:

$$S_{yy} = Y^*(f)Y(f) \tag{3-47}$$

Where: S_{yy} = autopower spectrum of signal $y(t)$

Like the linear spectrum, the autopower spectrum may be expressed in a one-sided form (i.e. only positive frequencies) or a two-sided form (i.e. positive and negative frequencies). The one-sided form is of greater practical significance, and it is defined as follows:

$$G_{yy}(f) = 0, \qquad f < 0 \qquad \text{(3-48a)}$$
$$G_{yy}(f) = S_{yy}(f), \qquad f = 0 \qquad \text{(3-48b)}$$
$$G_{yy}(f) = 2S_{yy}(f), \qquad f > 0 \qquad \text{(3-48c)}$$

Where: $G_{yy}(f)$ = one-sided autopower spectrum

The result is a real valued function equivalent to the magnitude of the linear spectrum squared. It is important to note that when the autopower spectrum is calculated, phase information is lost. This spectrum is useful in situations where amplitude vs. frequency information is required but phase is of little or no interest.

3.5.3 Time-Frequency Analysis

If the statistical properties and frequency content of a measurement signal have a strong dependence on the time interval of the analysis, the standard FFT may not be applicable. For example, if acceleration data are acquired from the surface of an engine block during a "sweep" through the engine's RPM range, there will be a number of components that "move" along the frequency axis because they are multiples of the crankshaft rotational speed. Standard FFT methods do not reveal which components are related to the operating speed of the engine. A time-frequency representation, on the other hand, reveals the temporal localization of a signal's spectral components. If the evolution of the spectral content with time is observed, it is possible to determine which

frequency components are related to the engine speed, and which components are related to structural vibration modes.

3.5.3.1 Short-Time Fourier Transform

A standard method used to investigate time-varying signals is the Short Time Fourier Transform (STFT). Practically speaking, the method involves selecting a relatively narrow observation period, applying a time window, and computing the frequencies in that range. The observation window then slides along the entire time signal to obtain a series of successive spectra. If the results are to be meaningful, the spectral characteristics of the signal must remain reasonably stationary over the duration of the window.

The STFT provides constant resolution in both the time domain and frequency domain. The "localization" characteristics of the analysis can be tuned by adjusting the length of the window function. The main drawback of this technique is that the window size is fixed throughout the transformation, and thus the low- and high-frequency components are analyzed with the same resolution.

The end result of the STFT is a 3-dimensional representation in which it is possible to observe the changes in both frequency content and amplitude with respect to time.

In the practice of analyzing engine vibrations, it is often desirable to take measurements over the course of an engine run-up in which the RPM is ramped gradually throughout the operating range of the engine. In this situation, the standard FFT is not applicable because frequency components that are related to the speed of the engine

(known as *orders*) will move along the frequency axis with changing RPM. If the FFT is applied to short, consecutive blocks of data in which the RPM is relatively constant, it is possible to view the evolution of frequency content with respect to engine RPM. Since engine RPM information is invariably collected during such run-up tests, it is possible to implement an algorithm in which a frequency spectrum is calculated at regular RPM intervals (for example every 25 or 50 RPM). This concept is illustrated in Figure 3.21.

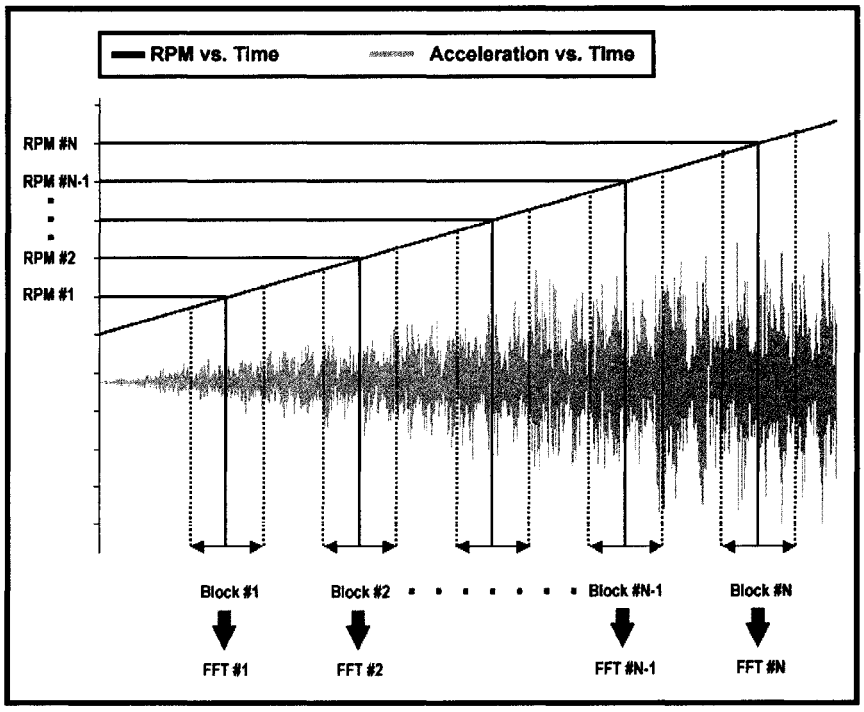

Figure 3.21: Generating frequency spectra at constant RPM increments.

3.5.4 Angle Domain Analysis

In simple terms, crankshaft angle domain analysis involves the observation of engine diagnostic signals as a function of crankshaft angle. The cyclic nature of internal combustion engine operation makes analysis of data in the crankshaft angle domain very

logical and useful because it allows one to correlate any observed signal abnormalities with specific points in the engine cycle.

3.5.4.1 Acquiring Angle Domain Data

There are two main techniques that may be used to obtain data in the crankshaft angle domain: *synchronous triggering* and *synchronous re-sampling*. As will be discussed in the following sections, each technique has certain advantages and disadvantages as well as specific areas of applicability.

3.5.4.1.1 Synchronous Triggering

Synchronous triggering refers to the use of a trigger signal to tell the data acquisition system when to take a data sample. For engine applications, this technique involves the use of an encoder signal that is position-locked to the crankshaft. If a toothed wheel is rigidly bolted to the flywheel, the trigger signal may be generated by a magnetic pickup that senses passage of the teeth on the wheel. Using this technique, the angle resolution is determined by the number of equally-spaced teeth on the wheel. Optical encoders are commercially available with varying levels of angle resolution, but these devices are generally very expensive. The primary advantage of using the synchronous triggering approach is that it provides accurate crankshaft angle domain data directly, with no further processing required. However, it is not always practical or possible to attach a toothed wheel or encoder to the engine flywheel to generate the trigger signal (for example, if the engine is installed in a vehicle). As well, for the toothed-wheel approach, the sample rate is limited by the number of teeth that can

accurately be machined onto the outer diameter of the wheel. Lastly, not all data acquisition systems provide the capability to continuously sample based on a trigger signal.

3.5.4.1.2 Synchronous Re-sampling

Synchronous re-sampling is a post-processing algorithm that transforms time domain data into the crankshaft angle domain using a tracking signal. A tracking signal is a voltage pulse that occurs a fixed number of times per crankshaft revolution. The system detects when the tracking signal voltage crosses a threshold value on the rising (or falling) slope, and then calculates instantaneous rotational speed based on the elapsed time between threshold crossings. Thus, using a tachometer signal, it is possible to generate an engine RPM vs. time function either in real-time during data acquisition, or in post processing. The RPM vs. time function may be numerically integrated to obtain the crankshaft angle vs. time function. It is the crankshaft angle vs. time function that is ultimately used in the transformation of data from the time domain to the crankshaft angle domain.

A constant target crankshaft angle resolution must be selected to define the time intervals at which data samples from the measurement signals should be available. This concept is illustrated in Figure 3.22.

From the required point in the angle domain α_I, the $\alpha(t)$ function is consulted to find the corresponding time instant (t_I). The value of the measured time signal at that instant (y'_I) must then be determined as the value for the angle position. This is repeated for every value in the angle domain. Depending on the resolution of the original signal

and the relation between both domains, interpolation may be required, as illustrated here. In order to maintain the dynamic nature of the signal, it is essential to preserve its spectral content, so the signal is first up-sampled before interpolation. As a final stage, the constructed angle domain signal needs to be re-sampled (usually down-sampled) to match the desired angle resolution. Preservation of the spectral characteristics during the up-sampling, interpolation, and down-sampling steps may require application of an appropriately designed low-pass finite impulse response (FIR) filter [34].

An obvious advantage of the synchronous re-sampling method is that it can be performed on time-based data that can be collected by any data acquisition system. Starting with standard time-based data, traditional time-domain and frequency-domain analysis may be performed in addition to angle-domain analysis. Another major advantage of this method is that, since it does not require any special implementations for data collection, it can be performed on data taken from engines that are installed in vehicles. Theoretically, the angle resolution that can be achieved is limited only by the sampling rate used to collect the original time-based data. Practically speaking, however, the accuracy of the results is extremely dependent on the quality of the tracking signal that is used to make the transformation. For constant RPM measurements, a reliable one pulse-per-revolution tracking signal is adequate for most purposes. For measurements performed during RPM sweeps (i.e. engine run-ups), it may be necessary to acquire a tracking signal that generates numerous pulses per crankshaft resolution to ensure positional accuracy.

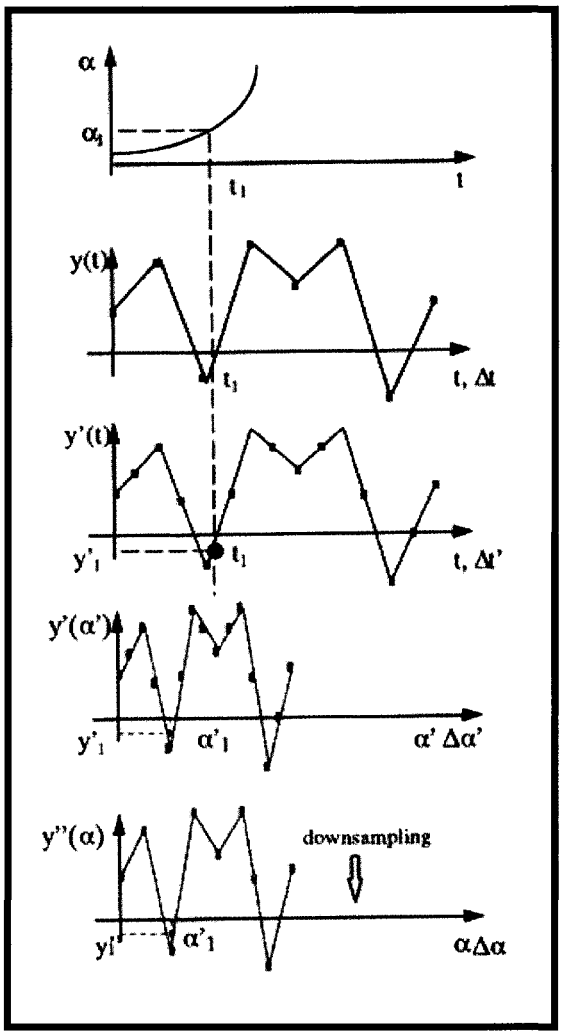

Figure 3.22: Synchronous re-sampling.

3.5.4.2 Variance Analysis

Variance analysis provides information about cycle-to-cycle variation during engine operation. If operating conditions are carefully controlled, and data are collected over a relatively short period of time, the acquired signals usually repeat qualitatively with a frequency that is directly proportional to the engine speed. Data based in the crankshaft angle domain are ideal for cycle-to-cycle comparisons because it can be ensured that data samples exist at the same points in each of the recorded cycles, and that

each block of data contains the same number of points. If a cycle reference signal is acquired simultaneously with the data, it can be used to "shift" the data along the crankshaft angle axis so that the angles correspond to known points in the actual engine cycle. A camshaft sensor signal is convenient to use for this purpose because the camshaft undergoes exactly one revolution per engine cycle.

Variance analysis consists of three distinct steps: ensemble averaging, running variance computation, and average variance computation. These steps will be described in the paragraphs that follow.

Ensemble averaging is the averaging of signal amplitudes for each individual crankshaft angle. Mathematically, it is applied as follows:

$$\bar{X}_\theta = \frac{1}{N}\sum_{i=1}^{i=N} X_{\theta,i} \tag{3-50}$$

Where: $\bar{X}_\theta$ = average signal amplitude at crank angle θ
N = number of engine cycles being averaged
$X_{\theta,i}$ = signal amplitude in i^{th} cycle at crank angle θ

Running variance is a measure of the deviation of the signal amplitude from the ensemble average, for each crank angle, on a cycle-by-cycle basis. It is computed using the following equation:

$$RV_{\theta,i} = \left(X_{\theta,i} - \bar{X}_\theta\right)^2 \tag{3-51}$$

Where: $RV_{\theta,i}$ = running variance in i^{th} cycle at crank angle θ

Finally, the *variance* is obtained as follows:

$$\sigma_\theta = \frac{1}{N}\sum_{i=1}^{i=N} RV_{\theta,i} \tag{3-52}$$

Where: σ_θ= variance at crank angle θ

Figure 3.23 graphically presents the steps involved in the computation of variance.

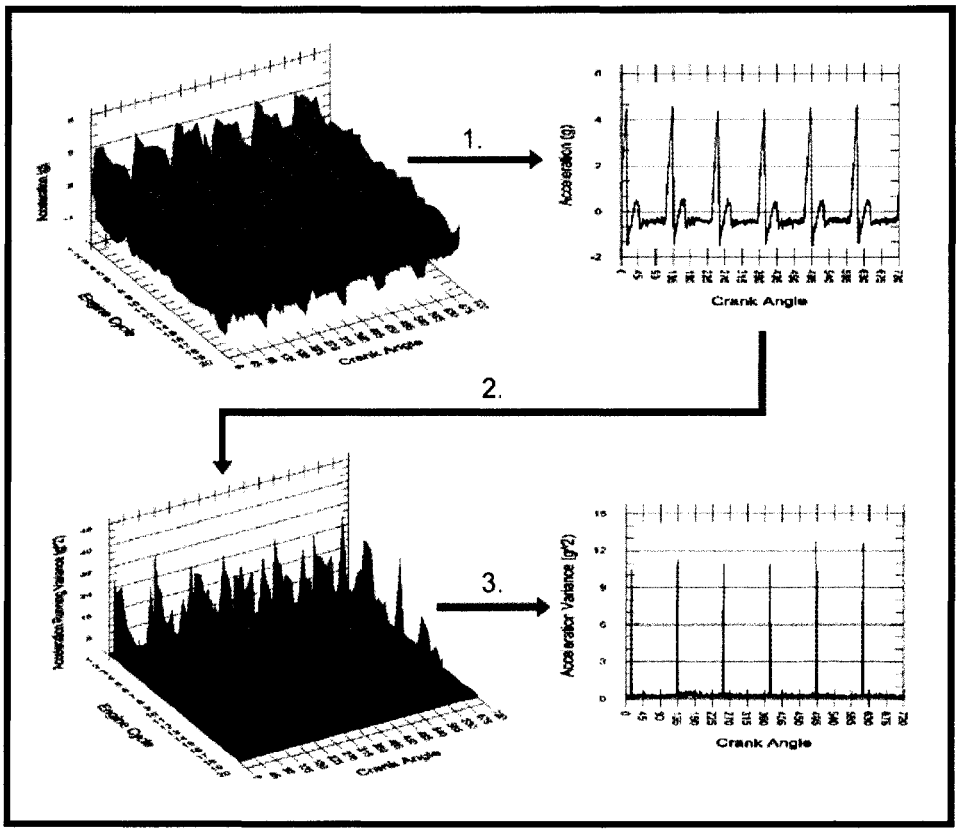

Figure 3.23: Computation of variance: (1) ensemble averaging; (2) running variance; (3) variance.

The most useful application of the variance technique is the extraction of localized vibration abnormalities. In particular, the method is very effective when attempting to isolate mechanical impact events. In the case of piston slap, an accelerometer may be placed on the exterior of the engine block, near the top of the cylinder, on the thrust side. Since the piston impacts the cylinder wall on the interior side, this accelerometer should easily detect the impact. Applying the variance technique to this data would then have the effect of *accentuating* the localized high vibration amplitudes (i.e. the impact event) and *suppressing* the lower amplitudes that are

characteristic of normal engine operation. If the angle-domain data has been properly shifted with respect to the cycle reference signal along the angle axis, it is possible to verify that the piston impact event is indeed occurring near top-dead-center in the affected cylinder.

Figure 3.24 shows variance plots of accelerometer data taken from the block of a V8 engine on the exterior of cylinders #7 and #8. This particular engine had groove-like machining defects in cylinder #7 on the thrust side.

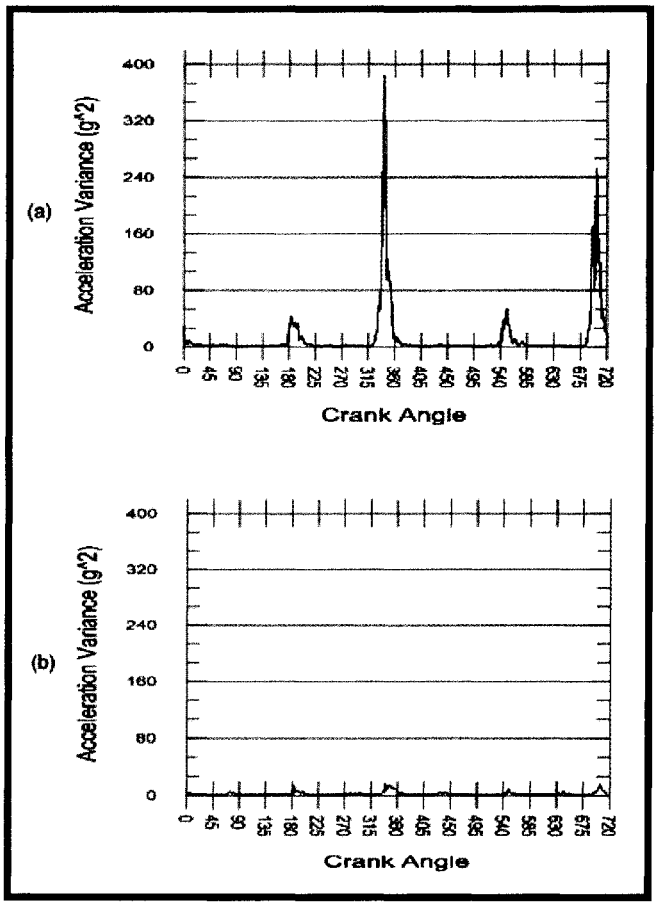

Figure 3.24: Variance plots of (a) cylinder #7 data and (b) cylinder #8 data.

The spikes that appear near 180° and 360° in the cylinder #7 variance plot seem to repeat near 540° and 720° respectively. These spikes correspond to the localized large-amplitude vibration that was caused by the piston rings coming into contact with the grooves. All of the spikes occur on downward strokes of the piston at exactly the same locations in the bore. The spikes also appear in the variance plot for cylinder #8 (albeit with much smaller amplitudes) because a vibration wave propagated from the point of excitation in cylinder #7 to the measurement point on the adjacent cylinder. This example illustrates how care must be taken when interpreting results because excitations occurring at all locations on the engine can propagate to a given measurement point and "cloud up" the results.

CHAPTER 4

EXPERIMENTAL DETAILS

4.1 Camshaft Chatter

The primary engine abnormality investigated in this study was a sound quality issue hereinafter referred to as *camshaft chatter.* The severity of camshaft chatter is dependent upon certain variables associated with the camshaft machining process. The phenomenon is a harsh, high-speed, metallic stuttering (i.e. chattering) sound that is present throughout the engine RPM range. The noise is most audible in the middle-RPM range under minimal engine load.

The chatter noise is caused by geometrical undulations on the camshaft lobes that excite valve train and cylinder head vibration modes during operation. The undulations are an artifact of the manufacturing process.

4.2 Engine and Camshafts

The engine used in this study was a spark ignition, 4-stroke, 3.0L Dual Overhead Camshaft (DOHC) V6. The engine was coupled to an AC engine dynamometer through a variable-ratio transmission.

For each bank of cylinders, DOHC engines employ one camshaft to operate the intake valves, and one camshaft to operate the exhaust valves. Exhaust camshafts were used in this study because of their better proximity to the available sensor-mounting locations. One of the camshafts used in this study is pictured in Figure 4.1.

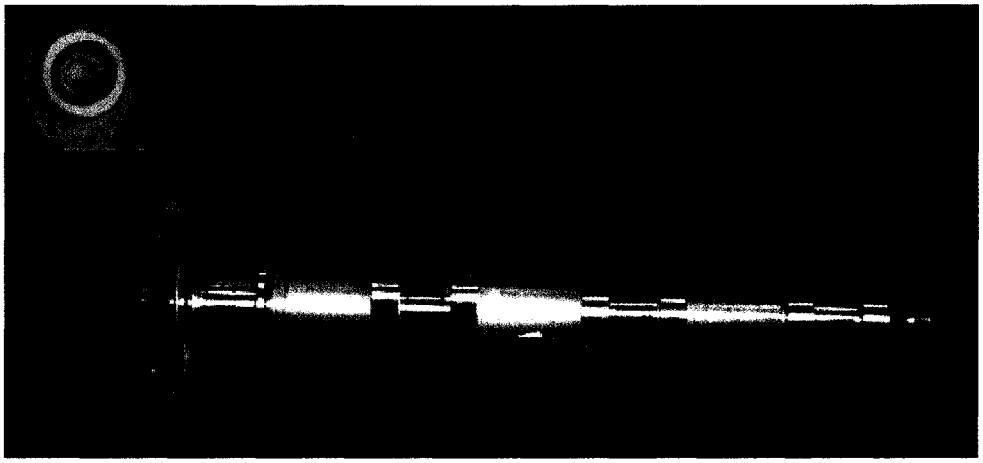

Figure 4.1: Example of DOHC V6 exhaust camshaft. The cam profile is shown in the inset.

Eight camshafts were tested, each one being subject to different combinations of machining parameters. A simple schematic of the machining process is shown in Figure 4.2. The parameters that were chosen, and the combinations that were used for the eight camshafts, are summarized in Table 4.1.

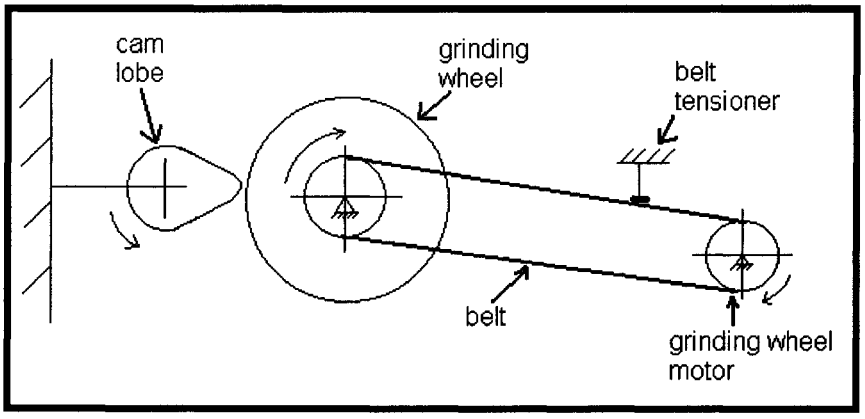

Figure 4.2: Schematic of camshaft machining process.

	GRIND WHEEL VIBRATION	CAM ROTATION SPEED	MOTOR VIBRATION	BELT TENSION	CLAMP PRESSURE
Cam #1	LOW	LOW	LOW	LOW	LOW
Cam #2	LOW	HIGH	LOW	LOW	HIGH
Cam #3	HIGH	LOW	HIGH	LOW	HIGH
Cam #4	LOW	LOW	LOW	HIGH	HIGH
Cam #5	HIGH	HIGH	LOW	HIGH	LOW
Cam #6	HIGH	LOW	HIGH	HIGH	LOW
Cam #7	HIGH	HIGH	HIGH	HIGH	HIGH
Cam #8	LOW	HIGH	HIGH	LOW	LOW

Table 4.1: Summary of the combinations of machining parameters used for the 8 camshafts.

The parameters in Table 4.1, and the values corresponding to the high and low settings, are defined as follows:

Grind Wheel Vibration:

Description: RMS vibration amplitude of grinding wheel during machining process.

LOW = 2.5×10^{-4} mm
HIGH = 7.6×10^{-4} mm

Cam Rotation Speed:

Description: Rotational speed of camshaft during machining process.

LOW = 19 RPM
HIGH = 60 RPM

Motor Vibration:

Description: RMS vibration amplitude of grinding wheel motor during machining process.

LOW = 1.3×10^{-4} mm
HIGH = 7.6×10^{-4} mm

Belt Tension:

Description: Tension of the grinding wheel drive belt during machining process.

Belt tension was not measured directly. It was varied between the "high" and "low" settings by adjusting the belt tensioner shown in Figure 4.2 to two different positions.

Clamp Pressure:

Description: Tightness of clamping of camshaft journals during machining process.

LOW = 225 psi
HIGH = 275 psi

4.3 Test Conditions – RPM and Load

For each camshaft, data were collected during sweeps from 1000 RPM to 5000 RPM. A ramp rate of 50 RPM/second was achieved via dynamometer and throttle control. The following load conditions were investigated:

1. Wide Open Throttle (WOT)
2. Part Throttle (PT)
3. Neutral / No Load (NL)

Data were also collected under constant-RPM idle conditions. Three measurement runs were performed for every camshaft/load combination.

4.4 Vibration Transducers

Two Dytran Model 3053B2 Tri-axial accelerometers (see Appendix A, Figure A.1 for specifications) were mounted on the left-side cylinder head of the test engine (Figure 4.1). One accelerometer was mounted near the front camshaft bearing, and the other was mounted near the rear camshaft bearing. The sensors were mounted using a strong adhesive to ensure good high-frequency response characteristics. The V6 test engine, with accelerometers mounted, is shown in Figure 4.3.

Figure 4.3: Full view (left) and close-up of V6 showing accelerometer locations (red circles).

4.5 Digital Engine Tachometer

To allow for subsequent order tracking and angle domain analysis, it was necessary to record the engine operating speed simultaneously with the vibration signals. To measure engine RPM, an Ono Sokki CT-6520 Digital Engine Tachometer with Ono

Sokki IP-292 primary ignition coil pick-up was used (see Appendix A, Figure A.2 for specifications).

The principal of operation of this device is as follows. The pick-up is clamped onto the wire powering the primary side of the engine's ignition coil. The current flowing in the primary coil is intermittent, with a frequency corresponding to the ignition events in the engine cylinders. The magnetic field that results from current flow in this wire induces voltage pulses in the inductive pick-up. The number of voltage pulses per engine revolution (3 for a V6), and a threshold voltage are set using controls on the digital tachometer unit. Essentially, the unit counts the voltage pulses and outputs a 5 V digital pulse once every engine revolution. This digital output is connected to the tachometer channel of the data acquisition system.

4.6 Data Acquisition Details

To ensure data consistency, the accelerometer channels were calibrated using a Bruel & Kjaer Calibration Exciter Type 4294 (see Appendix A, Figure A.3 for specifications).

Data was collected using a Unix-based LMS Cada-X system with a VXI front-end. The accelerometer signals (6 in total), and the engine tachometer signal, were digitized at a rate of 32767 samples per second.

The front-end was equipped with a built-in anti-aliasing filter that automatically adjusted to the selected sampling rate to ensure that aliased frequencies were not digitized.

CHAPTER 5

DATA ANALYSIS

There were three goals during the data analysis stage of this study:

1) To find a consistent means of detecting and characterizing the camshaft chatter phenomenon
2) To quantify the severity of camshaft chatter using an objective measure
3) To assess the relative dependence of camshaft chatter on the selected machining inputs

Obviously, it was necessary to achieve the first goal before even attempting to achieve the other two. Some of the techniques presented in Chapter 3 were employed in an attempt to extract the phenomenon from the vibration data. This chapter will describe the steps that were taken during the analysis stage of the study.

5.1 Analysis Methods

The following techniques were applied in an attempt to accomplish the three goals listed above.

1) Time Domain Data Comparison – As an initial check of the data, the measurement signals were compared in the time domain. Linear averaging of the signals was applied to reduce noise.

2) Overall RMS Vibration Comparison – To obtain a measure of vibration energy in each case, RMS vibration levels were computed at various engine speeds.

3) Angle Domain Variance – This technique was applied to investigate how the measurement signals varied with respect to the engine cycle.

4) *RPM-Frequency Analysis* – The most in-depth analysis of the data was performed during this stage. The Short Time Fourier Transform was used in an attempt to reveal the RPM-varying characteristics of camshaft chatter in the frequency domain. The measurement signals were played back through speakers to correlate audible phenomena with graphical representations.

5) *Band-Limited RMS Analysis* – After the frequency content of camshaft chatter was identified using RPM-Frequency analysis and audio feedback, RMS accelerations were computed on a limited band of frequencies to quantify the severity of the phenomenon.

6) *Main Effects Analysis* – This is an analysis method described by Breyfogle [54]. It was used to assess the relative dependence of camshaft chatter on each of the individual machining inputs.

5.2 Selection of Appropriate RPM and Load Conditions

As mentioned in Chapter 4, vibration data were collected during engine idle, as well as during run-ups from 1000 RPM to 5000 RPM, at 50 RPM/second, under the following load conditions:

1. Wide Open Throttle (WOT)
2. Part Throttle (PT)
3. Neutral / No Load (NL)

For the first two cases, the throttle was opened either fully (WOT) or partially (PT) at the start of the test run, and the linear ramp rate of 50 RPM/second was achieved via dynamometer load control. In order to perform the NL run-up, the RPM had to be

controlled via throttle opening as opposed to dynamometer control to achieve a true no-load condition.

After an initial investigation, it was found that the WOT data and the NL data were not as useful as the PT data. The WOT data exhibited a large influence of combustion noise, making camshaft chatter difficult to discern in some cases. The NL data contained comparatively much less combustion noise, but it was plagued with inconsistent RPM ramping owing to the fact that RPM was controlled via throttle as opposed to dynamometer load. This problem is clearly visible in Figure 5.1, which shows examples of RPM vs. Time curves for the three conditions.

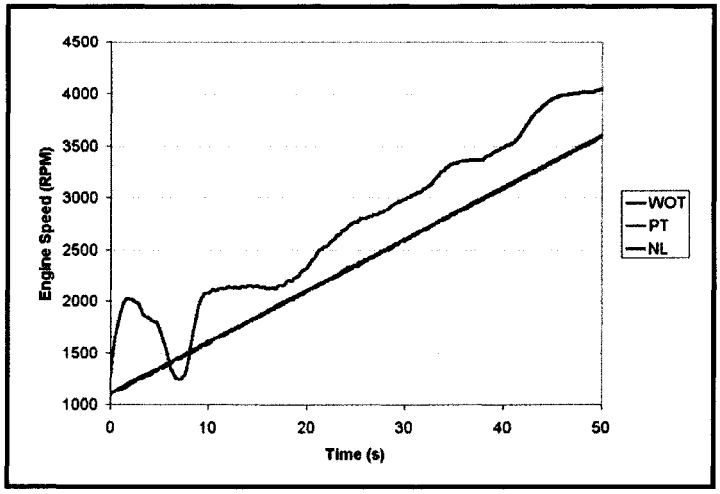

Figure 5.1: RPM vs. Time curves for WOT, PT, and NL conditions.

Ultimately, it was decided to proceed using the PT data only, since it represented a compromise between reduced combustion noise and accurate RPM control.

Results from three measurement runs were averaged for all analyses to obtain more realistic representations.

CHAPTER 6

RESULTS AND DISCUSSION

In this chapter, the data analysis methodology that was followed will be described, and the results will be presented and discussed. In most cases, the reader will be referred to appendices to view complete sets of results, as only representative examples have been included in this chapter for the sake of readability.

6.1 Time Domain Analysis

It was thought that a natural first step in the analysis would be to look at the measurement signals in the time domain to see if there were any noticeable, and possibly quantifiable, differences between the various camshafts.

When the raw data for the camshafts were compared on the same scale it was immediately apparent that more advanced methods would be required in order to distinguish between the camshafts. Since three measurement runs were performed for each camshaft/load combination, linear averaging was attempted as well. While this technique helped to remove some of the noise from the signals, it was still not possible to draw any meaningful conclusions.

6.2 RMS Analysis

A major problem with the aforementioned time domain comparison was that the sheer quantity of data associated with a single measurement run was rather overwhelming. It was surmised that the RMS parameter would be useful in comparing

the relative energy content between different signals, in a format that would be much easier to interpret.

RMS acceleration was calculated for 30 engine cycles at the following engine speeds: idle (approximately 720 RPM), 1500 RPM, 3000 RPM, and 4500 RPM. The results are shown in Figure 6.1.

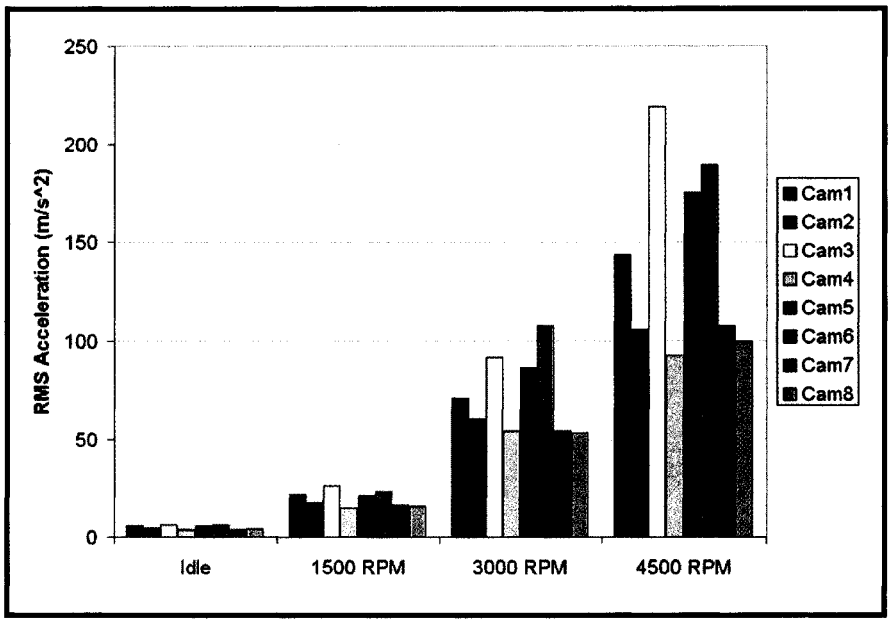

Figure 6.1: 30-cycle RMS acceleration for each camshaft at different engine speeds.

As was expected, the RMS vibration level increased with RPM. It can also be seen that the "ranking" of relative magnitude (i.e. from the highest down to the lowest) was fairly consistent throughout the RPM range. This simple analysis revealed the following useful information:

1. Vibration energy increased with increasing RPM
2. There were detectable differences between the different camshafts

3. The "ranking" of the camshafts was quite consistent throughout the RPM range

The RMS analysis was not expected to yield definitive answers, but rather, it was viewed as a preliminary comparison that could be used to support results obtained from more advanced analysis methods.

6.3 Variance Analysis

The next step in the analysis was computation of variance vs. crankshaft angle for each of the camshafts. In order to accomplish this, it was first necessary to synchronously re-sample the data to provide angle-domain information. For this part of the analysis, the engine's camshaft sensor (CID) was used as the tracking trace for the transformation to the angle domain. To ensure that the results were valid, a study was performed to verify the validity of this tracking trace. This study is described in Appendix B, and evidence of validity is presented.

A sample variance plot showing the prominent valve train events occurring in the vicinity of the accelerometer mounting locations is shown in Figure 6.2.

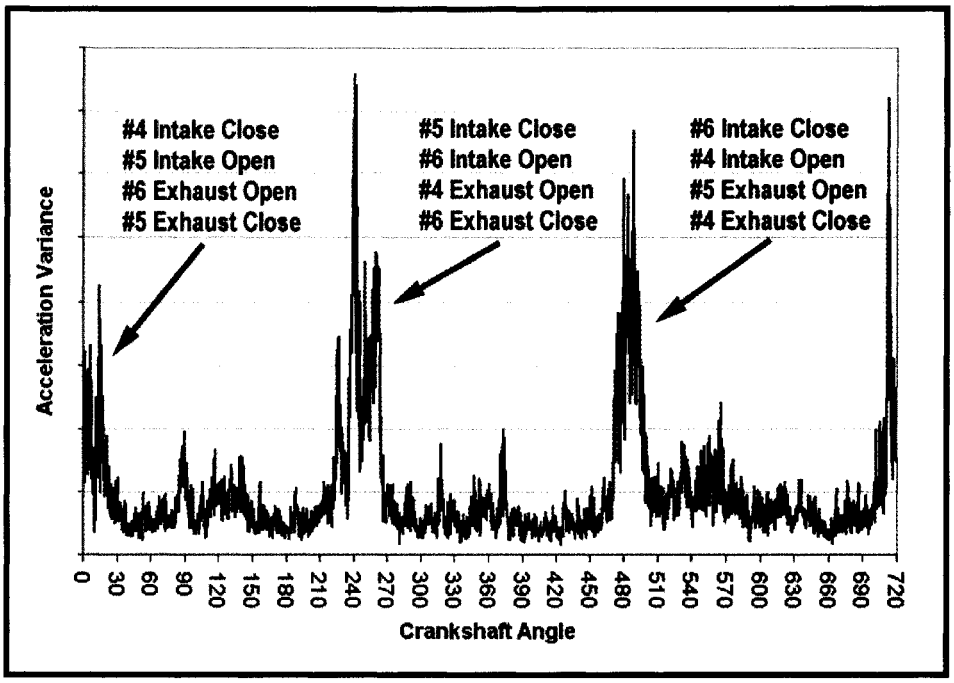

Figure 6.2: Example variance plot showing prominent valve train events (1500 RPM).

As mentioned in Chapter 4, the accelerometers were mounted on the left-hand-side cylinder head. The left-hand cylinder bank corresponds to cylinders #4, #5, and #6. As noted, each of the main spikes in Figure 6.2 corresponds to four major valve train events. In each case, the events are listed in order of occurrence. These events were occurring too closely together to be clearly distinguishable from each other.

In Chapter 3 it was noted that variance analysis is most applicable to data acquired under constant-RPM conditions. It was found that the character of the variance plot was extremely dependent on RPM. In Figure 6.3, variance plots are shown for 4 different engine speeds.

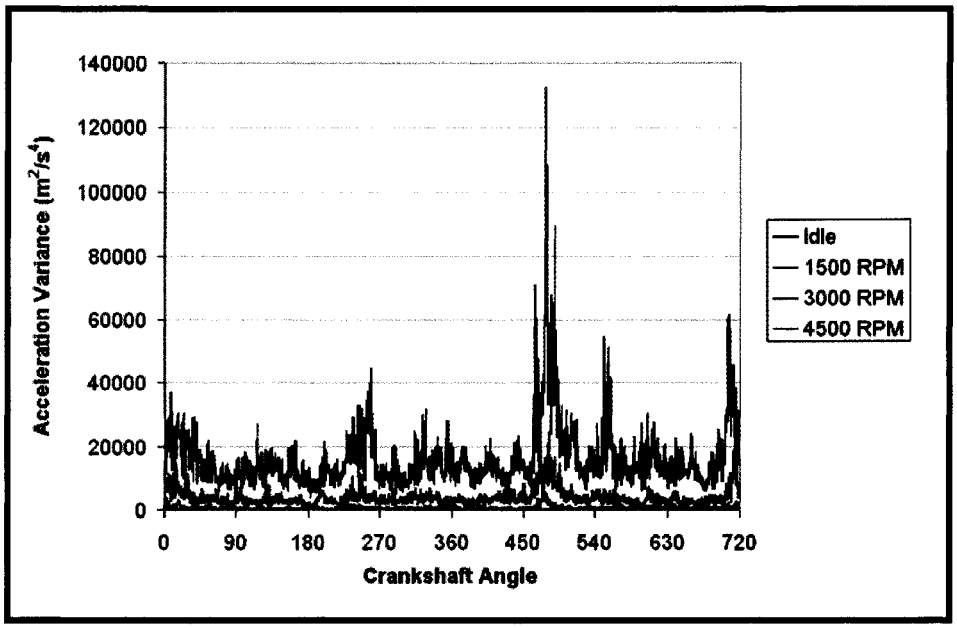

Figure 6.3: Evolution of variance with engine RPM.

The trend of increasing variance with increasing engine speed is clearly visible in the figure. This trend was observed for all of the camshafts tested. Increasing variance with increasing RPM suggests that as the engine speed rose, the data became more widely dispersed about the mean for each crankshaft angle. This was likely due to the increased frequency of valve train and combustion events. As can be seen from Figure 6.3, by the time 4500 RPM was reached, the signals were so "noisy" that the individual valve train events shown in Figure 6.2 were almost indistinguishable. Plots similar to Figure 6.3 can be found in Appendix C for each of the eight camshafts tested.

In Figure 6.4, variance plots associated with each of the eight camshafts under idle conditions are compared. Plots similar to Figure 6.4 for different RPM conditions can be found in Appendix D.

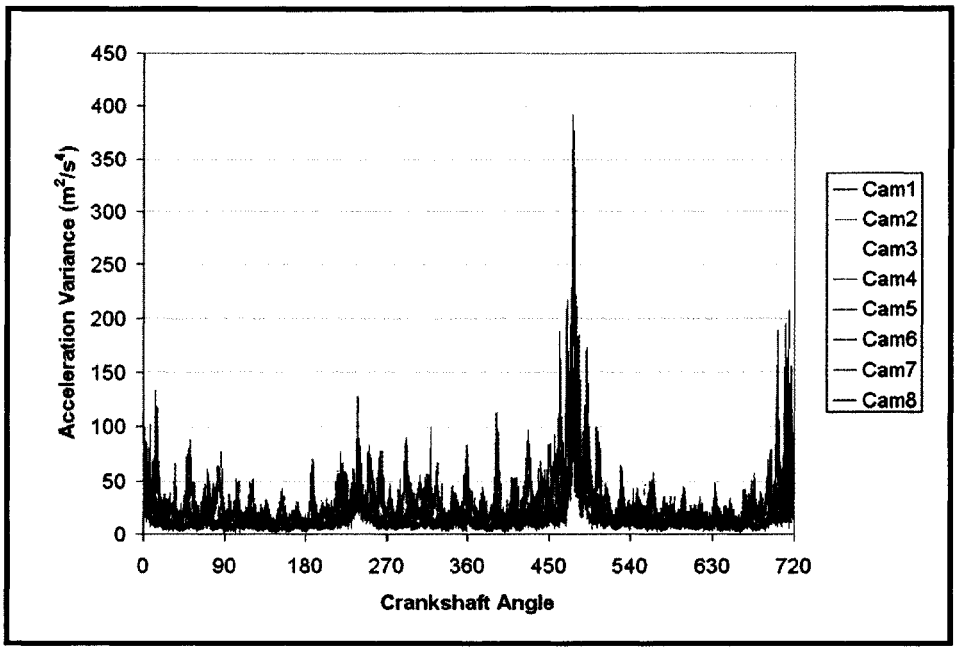

Figure 6.4: Comparison of variance for all 8 cams at idle (~ 720 RPM).

Upon observation of Figure 6.4 (and the other plots in Appendix D), differences between the variance plots for each of the camshafts were noticeable. However, it was ultimately decided that variance analysis was not a suitable tool for gauging the relative severity of camshaft chatter, since it is a measure of data dispersion as opposed to magnitude. In contrast to a mechanical impact event (such as piston slap), camshaft chatter is more of a *continuous* phenomenon that is not localized in the angle domain, meaning that variance analysis is only loosely applicable.

Nonetheless, variance analysis was a worthwhile step in this study, as it revealed the following information:

1. Valve train excitations were detectable from the chosen measurement locations
2. Dispersion of acceleration data about the mean increased with RPM for each crankshaft angle

6.4 RPM-Frequency Analysis

A major drawback of the RMS and variance analyses described in the previous two sections was that the data used contained information related to excitations that were not caused by the valve train or camshaft chatter. To address this problem, RPM-frequency analysis was applied in an attempt to characterize the frequency content of camshaft chatter.

6.4.1 Tracked Spectral Processing

The RPM-based Short Time Fourier Transform (STFT) described in Chapter 3 was applied to the run-up vibration data so that the evolution of frequency content with respect to RPM could be observed. Spectra were calculated every 25 RPM with a frequency resolution of 1 Hz. The resulting 3-dimensional plots associated with each of the eight camshafts turned out to be very similar to one another. A typical plot is shown in Figure 6.5. Plots for each of the eight camshafts can be found in Appendix E.

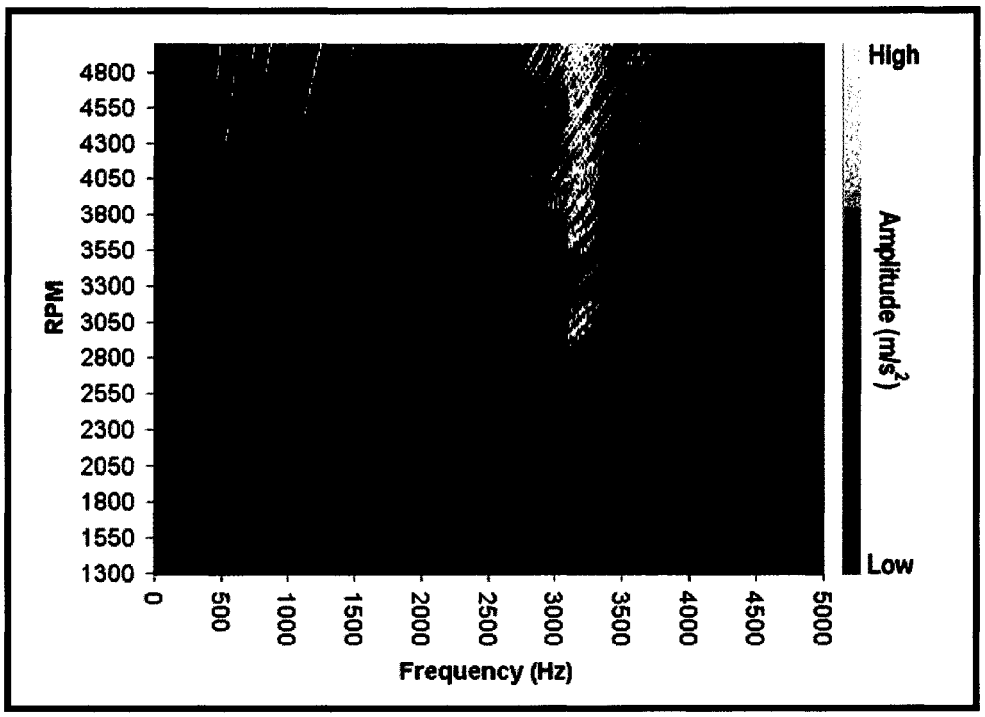

Figure 6.5: Color map showing the evolution of frequency content with RPM.

Two distinct classifications of frequencies are visible in Figure 6.5. Below approximately 2500 Hz, a series of radial lines dominates. These components – known as *orders* – are harmonics of engine speed so they increase in frequency with increasing RPM. A 1st order phenomenon happens exactly once per crankshaft revolution, a 2nd order phenomenon happens exactly twice per crankshaft revolution, and so on. In contrast, a series of components that remain stationary throughout the RPM range can be seen between approximately 3000 and 4000 Hz. These frequencies are associated with structural vibration modes, and as a result their location in the spectrum does not depend on RPM.

The band of frequencies between 3000 and 4000 Hz was suspected to be related to camshaft chatter. The technique described in the following section was used to investigate the validity of this assumption.

6.4.2 Audio Feedback of Measurement Signals

Using the LMS Cada-X software, it was possible to "play back" the acceleration signals through a speaker or headphones. This proved to be an invaluable tool in this stage of the analysis because it enabled one to literally listen for camshaft chatter and make subjective assessments regarding severity. Application of digital filtering in conjunction with audio feedback made it possible to precisely locate the phenomenon in the frequency domain. Audio feedback thus served to supplement graphical representations as evidence that camshaft chatter was being successfully characterized with respect to frequency content.

Two different digital filters were applied to all of the measurement signals before playback:

1. Band-pass filter with lower and upper cut-off frequencies of 3000 and 4000 Hz, respectively.
2. Band-stop filter with same cut-off frequencies as #1.

Since vibration energy above 5000 Hz was observed to be sparse, the important effect of the first filter was that it removed the dominating engine orders from the signals. The data shown in Figure 6.5 is repeated in Figure 6.6 - from 0 to 2500 Hz only – to show this part of the spectrum in greater detail.

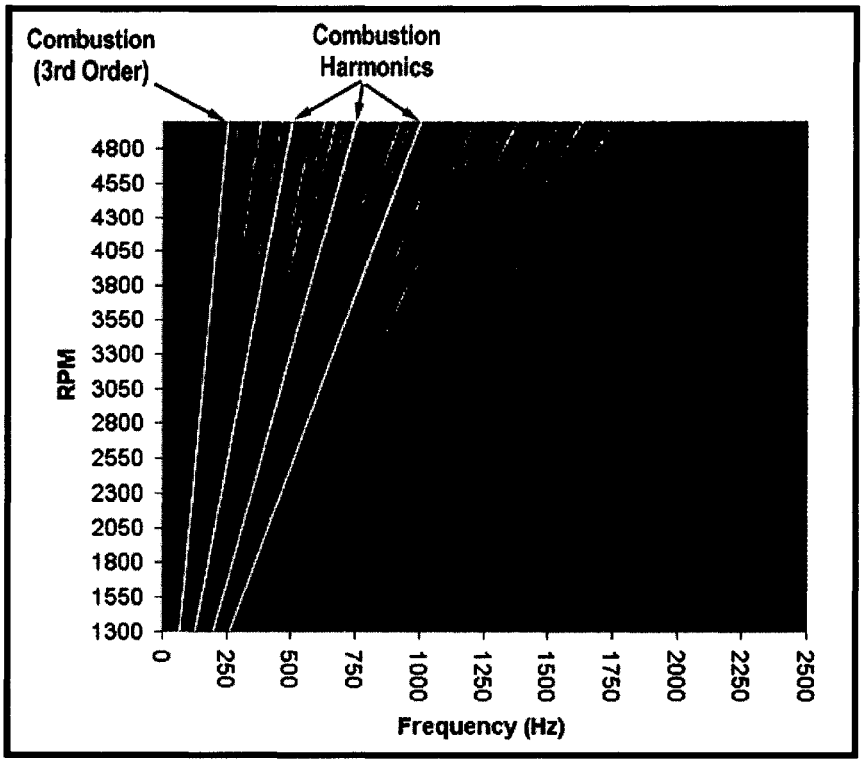

Figure 6.6: Color map showing 0 to 2500 Hz only.

The radial lines that are visible in this frequency range are spaced at half-order intervals. Since the 4-stroke cycle requires two crankshaft revolutions, it can be thought of as a 0.5 order occurrence. All major engine events tied to the engine cycle – such as valve train events - can then be expected to occur at multiples of 0.5 order. Combustion and its first three harmonics are highlighted in the figure. Combustion is a major source of both noise and variability, so filtering it from the acceleration signals helped greatly in isolating camshaft chatter.

As expected, the second filter had the inverse effect of the first – it essentially removed the camshaft chatter from the signals, while leaving the rest of the spectrum untouched.

6.5 Band-Limited RMS Analysis

After characterizing camshaft chatter with respect to frequency content, it was necessary to find a means of objectively assessing its severity. To obtain a measure of the energy present in the camshaft chatter "region" of 3000 to 4000 Hz, RMS analysis was applied to this band of frequencies only, and the results were plotted against RPM (Figure 6.7).

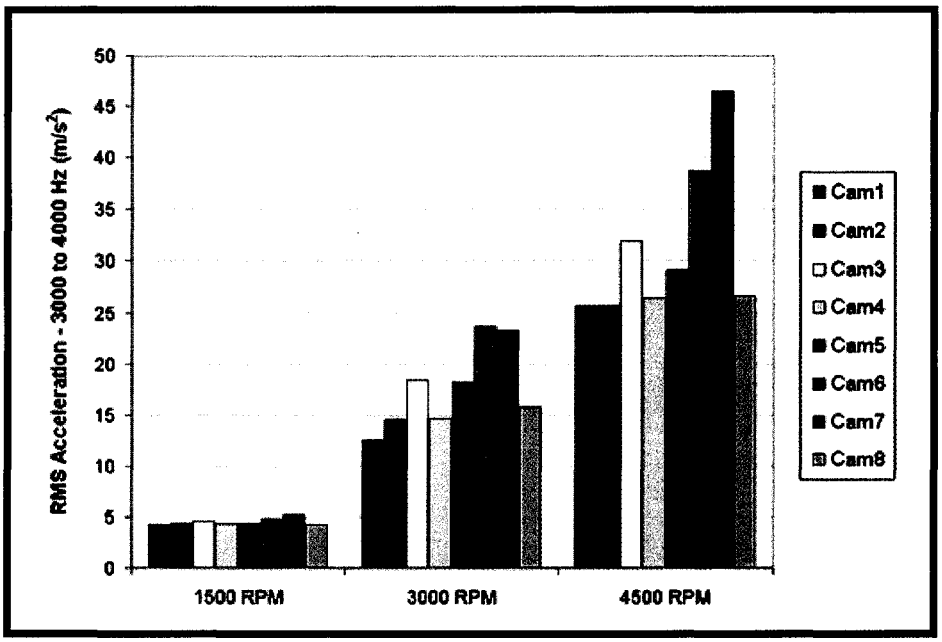

Figure 6.7: Band-limited RMS vibration for the eight camshafts.

The results of Figure 6.7 were considered to be the most meaningful of the study, since they were obtained following a detailed investigation into the nature of the camshaft chatter vibration response. Even though the presence of camshaft chatter in the region of 3000 to 4000 Hz was verified by graphical representation and corroborated by audio feedback, it could not be concluded that this phenomenon was the *only* excitation causing a response in this region. However, since the only thing changing from test to test was

the camshaft, it was assumed that all other excitations remained relatively constant throughout the testing stage. Based on this assumption, it was decided that the varying levels of energy observed in the chatter region were caused by fluctuations in chatter severity from camshaft to camshaft.

6.6 Assessing the Relative Impact of the Machining Inputs

At this point in the study, it was felt that goals #1 and #2 set out at the beginning of the analysis phase had been successfully met: 1) camshaft chatter could be consistently detected in the vibration measurements, and 2) the severity could be objectively quantified using the band-limited RMS analysis. To achieve the third and final goal of assessing the relative impact of the different machining parameters, a method described by Breyfogle [54] was applied.

The method involved the calculation of the so-called *main effects* of the experimental inputs on the observed outputs. Here, the inputs were the machining parameters associated with the camshafts, and the outputs were assumed to be the band-limited RMS accelerations at 1500, 3000, and 4500 RPM shown in Figure 6.7.

Referring back to Table 4.1, it can be seen that for each of the five machining inputs, half of the camshafts were subject to a "high" setting and the other half were subject to a "low" setting. The main effect of a given input is calculated as follows:

$$ME_A = \overline{X}_{A+} - \overline{X}_{A-} \qquad (6\text{-}1)$$

Where: ME_A = main effect of input A
$\overline{X}_{A+}$ = average output when A is set to HIGH
$\overline{X}_{A-}$ = average output when A is set to LOW

In such an analysis, the most significant inputs are designated as those that exhibit the largest main effects. Values close to zero indicate that the input does not significantly influence the output. The sign of the main effect reveals which of the settings (i.e. high or low) yields the preferred output. The size of main effect that is considered "large" depends on the specific application, so the values must be assessed on a relative basis.

In Appendix F, the individual main effects calculations can be found. The results are summarized in Figure 6.8.

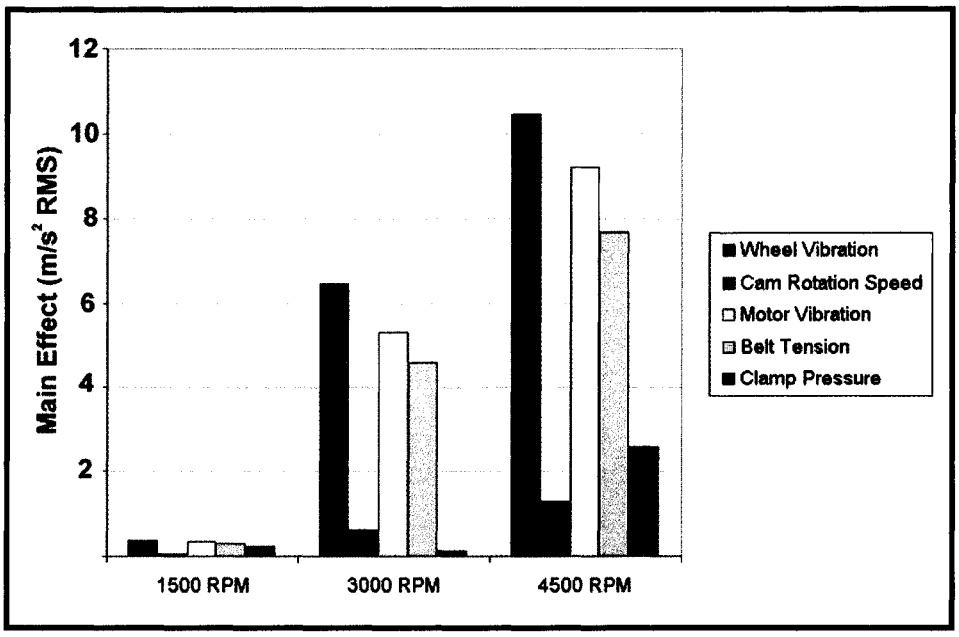

Figure 6.8: Main effects of the five machining inputs compared at three different engine speeds.

Looking at the figure, it can be seen that the machining inputs that had the greatest influence on camshaft chatter were Grinding Wheel Vibration, Motor Vibration, and Belt Tension. By comparison, Cam Rotation Speed and Clamp Pressure were shown to have little impact on the severity of camshaft chatter.

CHAPTER 7

CONCLUSIONS AND RECOMMENDATIONS

7.1 Conclusions

The following conclusions were reached after an in-depth analysis of the results:

1. The selected machining inputs had a strong effect on the vibrations caused by each of the camshafts. These effects were repeatable and remained intact throughout the RPM range.
2. The selected accelerometer mounting locations were very suitable for detecting camshaft chatter as well as all other important valve train events.
3. The influence of extraneous noise due to the frequency of valve train and combustion events increased considerably with RPM. For this reason, the mid-RPM range (i.e. approximately 3000 RPM) was considered to be the most crucial because it provided highly detectable excitations without excessive noise from other sources.
4. The frequency content of camshaft chatter consisted of a band of frequencies between 3000 and 4000 Hz. The phenomenon was present throughout the RPM range, but was most audible in the mid-RPM range under little or no engine load.
5. Grinding Wheel Vibration, Motor Vibration, and Belt Tension – in that order – were the most influential machining inputs. In all cases, the "low" setting showed lower levels of chatter severity.
6. Cam Rotation Speed and Clamp Pressure were shown to have a negligible effect on the severity of camshaft chatter.

7.2 Recommendations

The author makes the following recommendations to individuals or groups wishing to further investigate the impact of machining on camshaft chatter or, in general, vibrations related to camshafts and valve trains:

1) There was only one camshaft manufactured for each set of machining inputs. A more powerful approach would be to manufacture numerous parts with each set of inputs to verify the repeatability of the end results.
2) Tests similar to the ones described in this thesis should be performed without engine combustion, using a dynamometer to drive the engine at the required speeds (i.e. a *motoring* condition). This approach would eliminate the variability associated with combustion, and greatly reduce extraneous excitations.
3) An advanced computer model should be developed to simulate valve train dynamics. Such a simulation could help reveal the details of valve train excitations, and determine the salient mechanisms affecting sound quality.

REFERENCES

[1] R. S. Figliola and D. E. Beasley (1995). "Theory and Design For Mechanical Measurements", John Wiley & Sons, Inc., USA

[2] A. J. Wheeler and A. R. Ganji (1996). "Introduction to Engineering Experimentation", Prentice Hall, Inc., New Jersey, USA

[3] D. J. Ewins (1986). "Modal Testing: Theory and Practice", Research Studies Press Ltd., Great Britain

[4] R. B. Randall (1987). "Frequency Analysis", Research Studies Press Ltd., Great Britain

[5] R. Pallas-Areny and J. G. Webster (1991). "Sensors and Signal Conditioning", John Wiley & Sons, Inc., USA

[6] R. C. Eisenmann and R. C. Eisenmann Jr. (1998). "Machinery Malfunction Diagnosis and Correction", Prentice Hall, Inc., New Jersey, USA

[7] Harris and Crede (1976). "Shock and Vibration Handbook", McGraw-Hill Inc., USA

[8] H. Austerlitz (1991). "Data Acquisition Techniques Using Personal Computers", Academic Press, Inc., California, USA

[9] V. K. Madisetti and D. B. Williams (1998). "The Digital Signal Processing Handbook", CRC Press, Florida, USA

[10] D. Anderton and J. H. Zheng (1993). "A New Measurement Method For Separating Airborne and Structure Borne Sound From an I.C. Engine's Valve Train Mechanism", SAE Paper 931335

[11] M. Chien (1995). "Engine Impact Noise Measurement and Quantification", SAE Paper 951236

[12] J. W. Forbes et al. (1995). "Engine Knock Control via Optimization of Sensor Location", SAE Paper 951237

[13] H. Kamp and J. Spermann (1995). "New Methods of Evaluating and Improving Piston Related Noise in Internal Combustion Engines", SAE Paper 951238

[14] T. Onsay (1995). "The Use of Wavelet Transform and Frames in NVH Applications", SAE Paper 951364

[15] I. Suh and R. H. Lyon (1999). "An Investigation of Valve Train Noise for the Sound Quality of I. C. Engines", SAE Paper 1999-01-1711

[16] J. Bendat and A. Piersol (1971). "Random Data: Analysis and Measurement Procedures", Wiley-Interscience, New York, USA

[17] C. E. Summers (1925). "Measurement of Engine Vibration Phenomena", SAE Paper 250005

[18] L. R. Hulls and J. R. Welch (1967). "Engine Vibration Signals as an Aid to Fault Diagnosis", SAE Paper 670872

[19] R. C. Meier Jr. and T. G. Goetz (1985). "Cost-Effective Engine Diagnostics for Production Engine Hot Test", SAE Paper 851564

[20] J. Ben-Ari and G. deBotton (1999). "Fault Detection in Internal Combustion Engines by the Vibrations Analysis Method", SAE Paper 1999-01-1223

[21] A. Ball, F. Gu and W. Li (2000). "The Condition Monitoring of Diesel Engines using Acoustic Measurements", SAE Paper 2000-01-0368

[22] Z. Zhang and E. Tomota (2000). "A New Diagnostic Method of Knocking in a Spark-Ignition Engine Using the Wavelet Transform", SAE Paper 2000-01-1801

[23] C. Torrence and G. Compo (1998). "A Practical Guide to Wavelet Analysis", American Meteorological Society

[24] G. Galinsky (1994). "Air-Independent Diesel Combustion Noise", Master's Thesis

[25] L. Bell and D. Bell (1994). "Industrial Noise Control: Fundamentals and Applications", Marcel Dekker, Inc., New York, USA

[26] D. J. Inman (1996). "Engineering Vibration", Prentice-Hall, Inc., New Jersey, USA

[27] J. Tjong (1992). "Engine Dynamic Signal Monitoring and Diagnostics", Ph. D. Dissertation, University of Windsor, Windsor, Ontario, Canada

[28] S. G. Braun and B. B. Seth (1977). "Signature Analysis Methods and Applications For Rotating Machines", ASME 77-WA/Aut-5

[29] S. G. Braun and B. B. Seth (1980). "Analysis of Repetitive Mechanism Signatures", Journal of Sound and Vibration

[30] M. Serridge and T. Licht (1987). "Piezoelectric Accelerometer and Vibration Preamplifier Handbook", Brüel & Kjær

[31] J. T. Broch (1984). "Mechanical Vibration and Shock Measurements", Brüel & Kjær

[32] R. Stone (1992). "Introduction to Internal Combustion Engines", SAE, Warrendale, PA

[33] H. Heisler (1995). "Advanced Engine Technology", SAE, Warrendale, PA

[34] J. R. Blough and G. D. Gwaltney (1999). "Summary and Characteristics of Rotating Machinery Digital Signal Processing Methods", SAE Paper 1999-01-2818

[35] In-Soo Suh (2002). "Application of Time-Frequency Representation Techniques to the Impact-Induced Noise and Vibration from Engines", SAE Paper 2002-01-0453

[36] R. L. Stene et al. (1998). "Analyzing Vibrations in an IC Engine Valve Train", SAE Paper 980570

[37] G. deBotton et al. (2002). "Online Detection of Cylinder-to-Cylinder Variations by a Vibration Analysis System", SAE Paper 2002-01-0848

[38] E. Kamiyama and S. Yasuhara (1991). "Improvement of DOHC Valve Train Noise by Analysis of Valve and Tappet Movement", SAE Paper 911061

[39] M. Sopouch et al. (2002). "Simulation of Engine's Structure-Borne Noise Excitation Due to the Timing Chain Drive", SAE Paper 2002-01-0451

[40] M. Teodorescu et al. (2002). "Experimental Analysis of Dynamics and Friction in Valve Train Systems", SAE Paper 2002-01-0484

[41] A. Druschitz and S. Thelen (2002). "Induction Hardened Ductile Iron Camshafts", SAE Paper 2002-01-0918

[42] U. Kramer and P. Philips (2002). "Phasing Strategy for an Engine With Twin Variable Cam Timing", SAE Paper 2002-01-1101

[43] R. Rego and J. Martins (2001). "Valve Motion Modelation For Use in Airflow Engine Simulation", SAE Paper 2001-01-3958

[44] K. Akiba (2001). "A Study on Mode Analysis of SOHC Mechanism", SAE Paper 2001-08-0216

[45] B. Jawad et al. (2000). "Engine Control Inputs and Signal Conditioning for Crankshaft and Camshaft Positioning", SAE Paper 2000-01-3092

[46] R. Keribar (2000). "A Valvetrain Design Analysis Tool With Multiple Functionality", SAE Paper 2000-01-0562

[47] M. Stephenson et al. (2000). "A Simple Method For the Prediction and Cancellation of Camshaft Torque Fluctuations", SAE Paper 2000-01-0908

[48] H. Isaac Du and J. Chen (2000). "Dynamic Analysis of a 3D Finger Follower Valve Train System Coupled With Flexible Camshafts", SAE Paper 2000-01-0909

[49] B. Christenson et al. (1999). "Applied Development and Benefits of Camshaft Torsional Dampers", SAE Paper 1999-01-1861

[50] R. Norton et al. (1999). "Effect of Valve-Cam Ramps on Valve Train Dynamics", SAE Paper 1999-01-0801

[51] Y. Miura and S. Nakamura (1998). "Gear Rattling Noise Analysis For a Diesel Engine", SAE Paper 984089

[52] R. Norton (1988). "Effect of Manufacturing Method on Dynamic Performance of Cams – Part I", Mechanism and Machine Theory, 23(3), pp. 191-200

[53] R. Norton (1988). "Analysis of the Effect of Manufacturing Methods and Heat Treatment on the Performance of Double Dwell Cams", Mechanism and Machine Theory, 23(6), pp. 461-473

[54] F. W. Breyfogle (1999). "Implementing Six Sigma: Smarter Solutions Using Statistical Methods", John Wiley & Sons, Inc., USA

[55] J. Cooley and J. Tukey (1965). "An Algorithm for the Machine Calculation of Complex Fourier Series", Math. of Comp., Vol.19, No. 90, pp. 297-301.

APPENDICES

APPENDIX A:

EQUIPMENT SPECIFICATIONS

Specification	Value
Weight	7.5 grams
Sensitivity (-10% +15%)	10 mV/g
Full Scale Range (each axis)	+/- 500 g
Frequency Range +/- 10%	2 Hz to 5000 Hz
Maximum Vibration	+/- 600 g
Temperature Range	-60 to +250 °F
Supply Current Range (each axis)	2 to 20 mA
Supply Voltage Range (each axis)	+18 to +30 VDC
Discharge Time Constant	0.5 sec

Figure A.1: Specifications for Dytran 3053B2 Tri-axial accelerometer.

Specification	Value
Applicable sensors	IP-292/296/3000, OM-200, VP-201/202, MP-910/981, LG-916, TTL Fiber Sensor (Option)
Measurement Range	400 to 20000 RPM
Input Pulse Count	0.5 to 199.5 Pulses/Rev
Trigger Level	IP-292/296/3000, VP-202 and OM-200: adjusted by adjustment knob. Others: semi-fixed internally
Display	Green LED (5 digits) 14 mm character length
Measurement Range	Automatic repetition for each second
Reference Oscillator	Crystal
Oscillating Frequency	16 MHz
Precision	+/- 100 x 10^{-6}
Display Precision	400 to 20000 RPM (+/- 0.02% of full scale)
Output Voltage	0 to 10 V
Linearity	+/- 0.5% of full scale
Output Adjustment Range	+/- 4% of full scale (zero and span)
Response	approx. 80 ms or less
Data Output	Positive logic, TTL level, fan out of 2
Output Pulse Count	1 pulse/rev, 60 pulse/rev
Power Supply	100 VAC +/- 10%, approx. 25 VA (AC power), 11 to 15 V, approx. 13 V (DC power)
Operating Temperature Range	0 to +40 °C
Dimension	210 (W) x 99 (H) x 300 (D) mm
Weight	approx. 3 kg

Figure A.2: Specifications for Ono Sokki CT-6520 Digital Engine Tachometer.

Specification	Value
Vibration System	Electromagnetic exciter with internal built-in piezoelectric accelerometer for servo regulation of vibration amplitude
Frequency	159.2 Hz (1000 rad/s) +/- 1%
Acceleration	10 m/s^2 (RMS) +/- 3%
Velocity	10 mm/s (RMS) +/- 4%
Displacement	10 μm (RMS) +/- 5%
Transverse Amplitude	less than 5% of main axis amplitude
Distortion	less than 3%
Maximum Accelerometer Mass	70 g
Temperature Range	+10 to +40 °C
Humidity	Up to 90% relative humidity, non-condensing
Built-in Battery	9V alkaline

Figure A.3: Specifications for Bruel and Kjaer Type 4249 Calibration Exciter.

APPENDIX B:

VERIFICATION OF VALIDITY OF CID TRACKING

B.1 Verification of Validity of CID Tracking

This appendix describes a study that was performed to assess the validity of synchronous re-sampling using the engine's camshaft identification sensor (CID) as the tracking trace. In general, the synchronous re-sampling method of obtaining angle domain data is the preferred method because it does not require any special equipment during testing. The alternative to synchronous re-sampling, known as synchronous sampling, requires that a toothed wheel be rigidly attached to the engine crankshaft so that a magnetic pickup may detect passage of the teeth to trigger data acquisition at known points in the engine cycle.

CID tracking was investigated under the following conditions:

1. Constant RPM (idle)
2. Constant RPM (4000 RPM)
3. Ramp from 1500 RPM to 4500 RPM at approximately 150 RPM/second
4. Transient 'throttle blip'

For #4, the engine was running at idle and midway through the data acquisition the throttle was suddenly fully opened. The purpose of this was to determine the tracking ability of the CID signal during a rapid transient increase in RPM.

The engine that was used in this study had a verified rough machining defect in cylinder #6. Signals were acquired from the following sensors for this experiment:

1. Camshaft Identification Sensor (CID)
2. Crankshaft Position Sensor (CPS)
3. Piezoelectric Accelerometer mounted on cylinder #6

The CPS is a variable reluctance sensor that detects the passage of teeth on a wheel that is attached to the crankshaft. The teeth on the wheel are equally spaced to accommodate 36 teeth, but one tooth is missing to signify top-dead-center of cylinder #1. The CPS signal

is used in engine electronic control strategies to track the position of the crankshaft. The CID and CPS signals are shown together in Figure B.1 for one complete engine cycle.

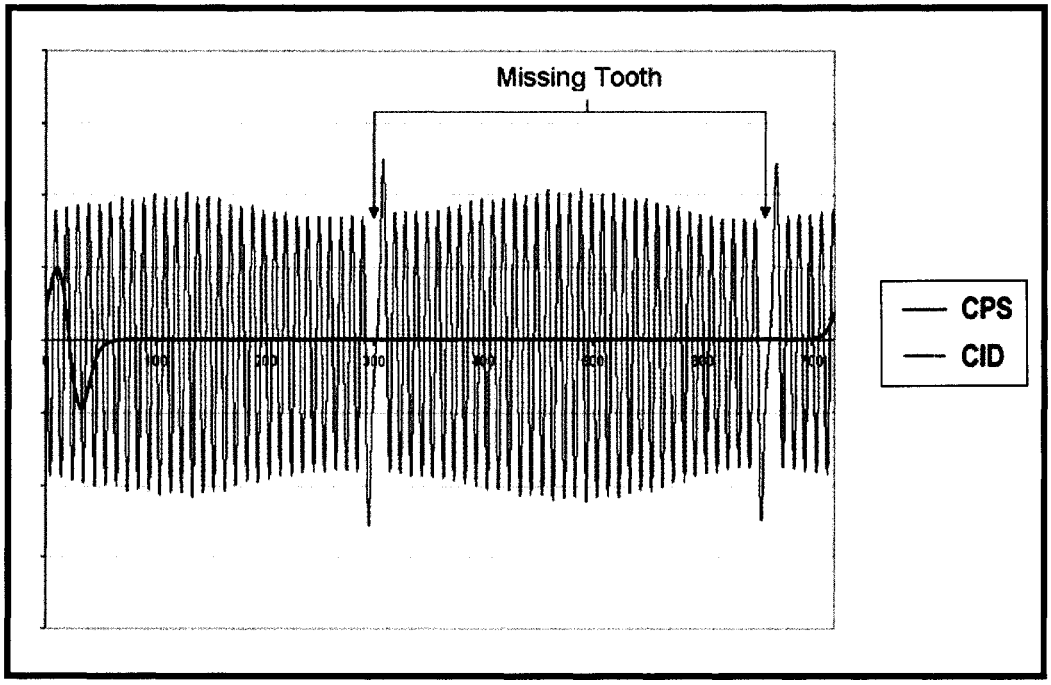

Figure B.1: CPS and CID signals for one engine cycle.

Due to the characteristics of variable reluctance sensors, the precise details of the signals generated by the CPS and CID vary slightly with engine RPM, but the important characteristics remain intact throughout the RPM range. The CPS signal was acquired because it is known how the signal should appear over the course of an engine cycle, and it can thus be used to verify whether or not the CID signal provides adequate tracking for transformation to the crankshaft angle domain. The accelerometer signal was acquired as an additional check to see if an actual vibration abnormality could be detected and successfully transformed to the angle domain.

As a first check, the CPS signal was transformed to the angle domain and broken down into individual engine cycles (i.e. 720° blocks). The cycles of data for each operating condition were averaged together to verify that the important characteristics of the signal were preserved. The results are shown in Figure B.2.

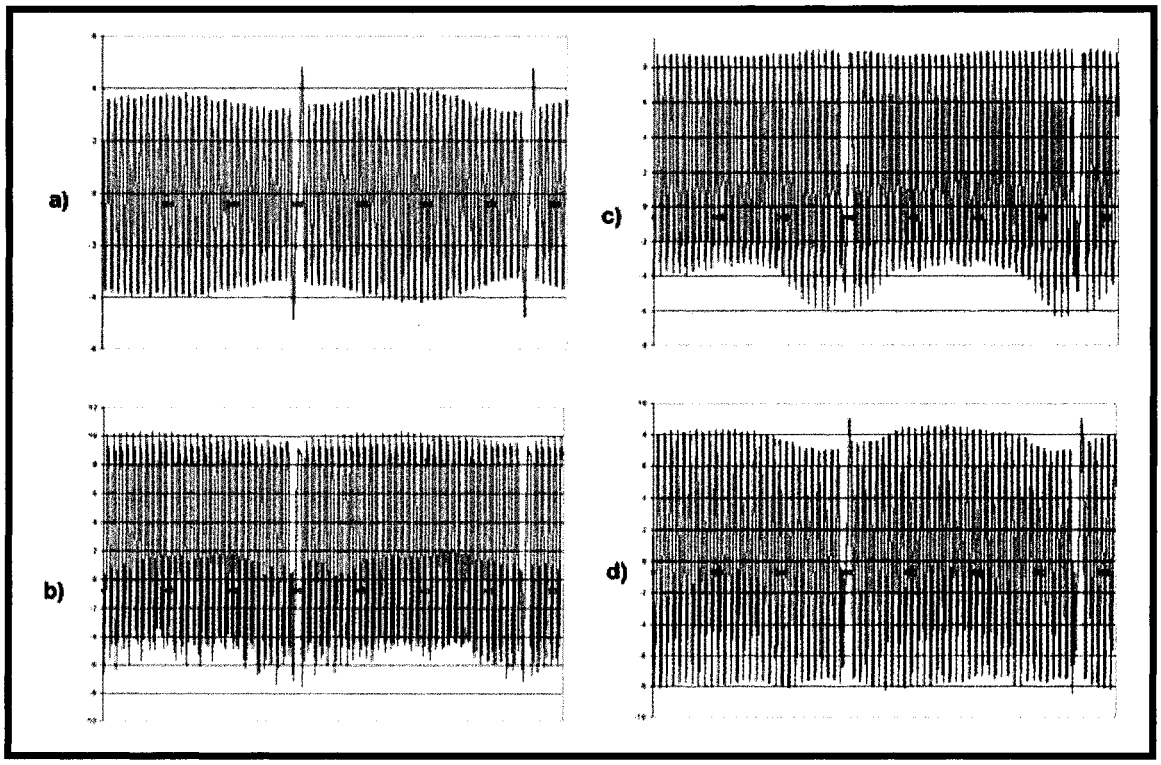

Figure B.2: CPS averages for a) idle; b) 4000 RPM; c) RPM ramp; d) transient throttle blip.

In each of the plots shown in Figure B.2, the 35 spikes and 1 gap per crankshaft revolution are clearly recognizable.

In Figure B.3, a short segment of the raw cylinder #6 acceleration signal is shown with the CID signal as a cycle reference. There are four regions indicated in the figure exhibiting abnormally high vibration amplitudes as a result of the piston rings coming into contact with the poorly machined surfaces within the cylinder.

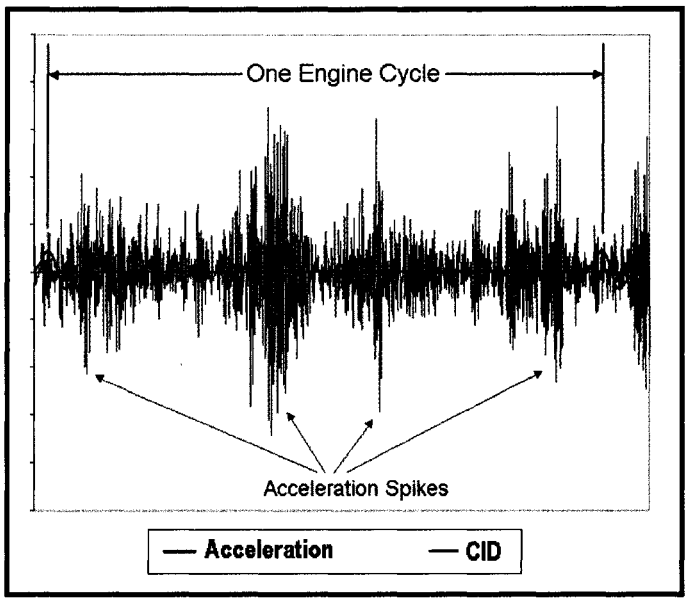

Figure B.3: Acceleration signal acquired from vicinity of defective cylinder.

Using the CID tracking trace, the data was transformed to the angle domain for each of the operating conditions. In an attempt to detect the defect, variance analysis was performed on the angle domain data. The results are shown in Figure B.4.

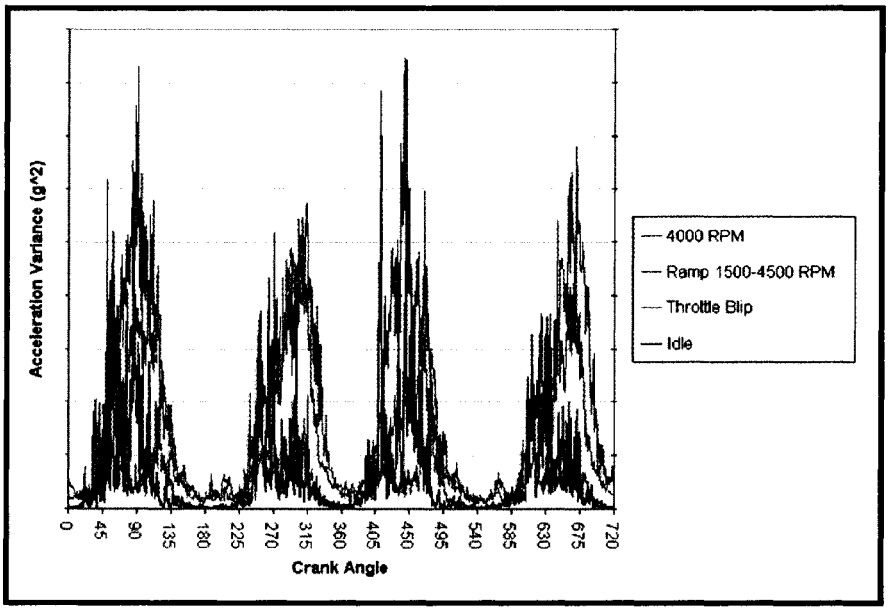

Figure B.4: Variance plots for each of the investigated conditions.

The results shown in Figure B.2 suggest that CID tracking is sufficient to accurately resolve an event that repeats itself 36 times per crankshaft revolution (i.e. a 36^{th} order event). In the crankshaft angle domain, the author is primarily interested in the ability to detect low-order events that are in some way tied to the engine cycle (such as valve impacts). The evidence presented here indicates that the CID signal is an adequate tracking trace for these purposes.

Additional evidence to support this claim can be seen in Figure B.4. The variance peaks appear at the same crankshaft angles for all of the conditions investigated. The peaks vary in amplitude and width, but this is due to the fact that the data was acquired at different engine operating speeds. The higher speeds resulted in higher levels of vibrational energy that took longer periods of time to dissipate.

APPENDIX C:

EVOLUTION OF VARIANCE WITH RPM FOR ALL CAMSHAFTS

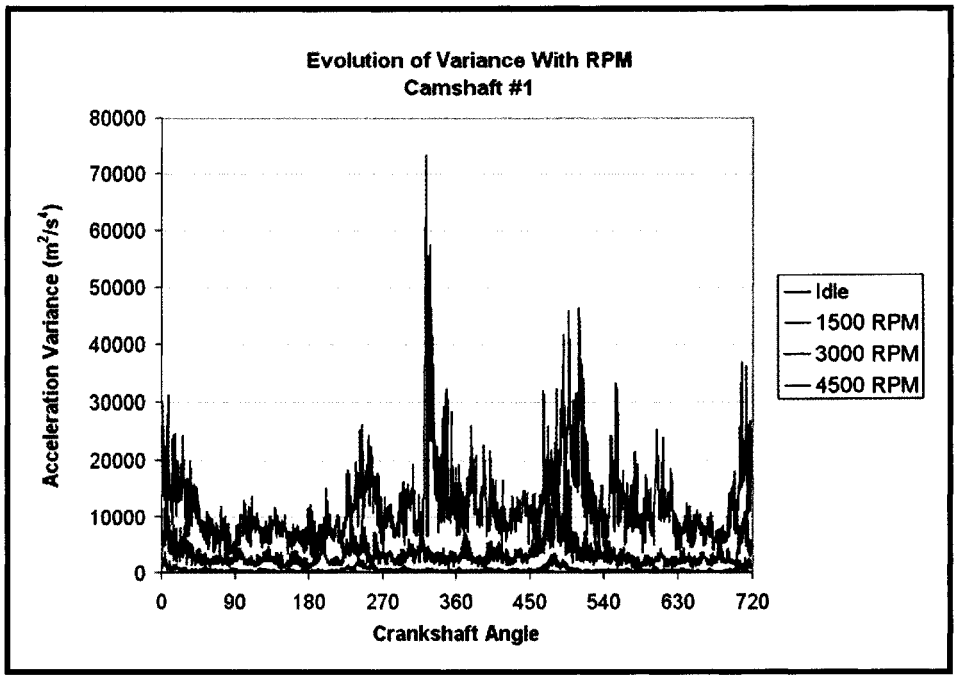

Figure C.1: Evolution of variance with RPM for camshaft #1.

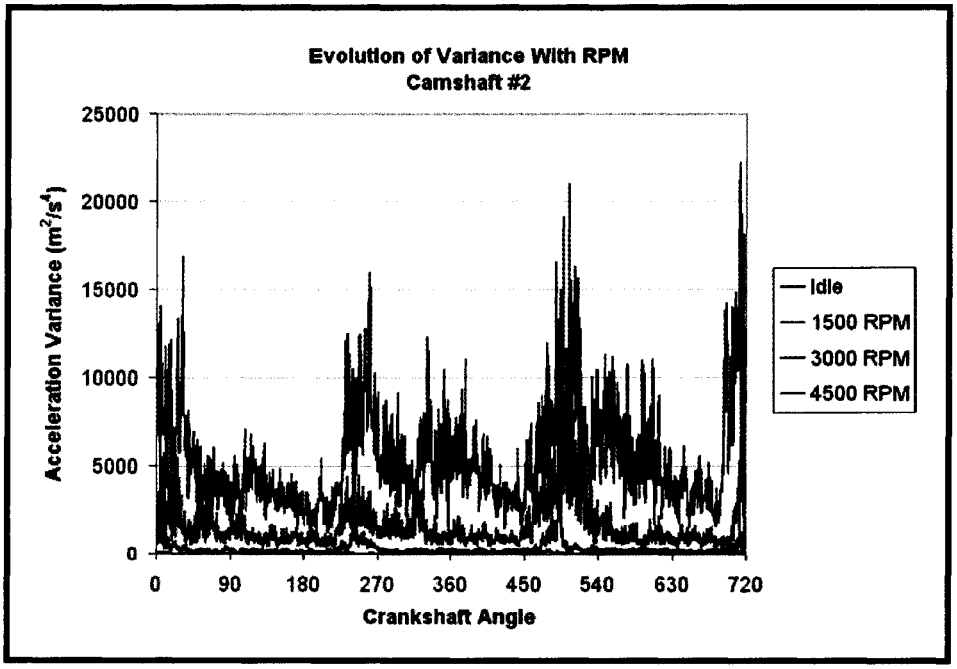

Figure C.2: Evolution of variance with RPM for camshaft #2.

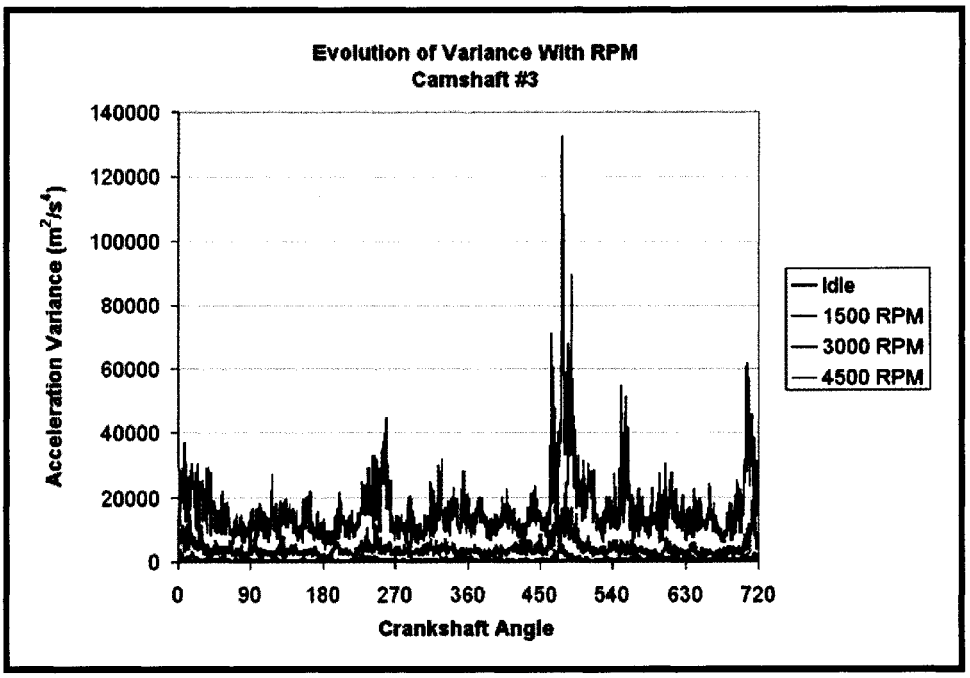

Figure C.3: Evolution of variance with RPM for camshaft #3.

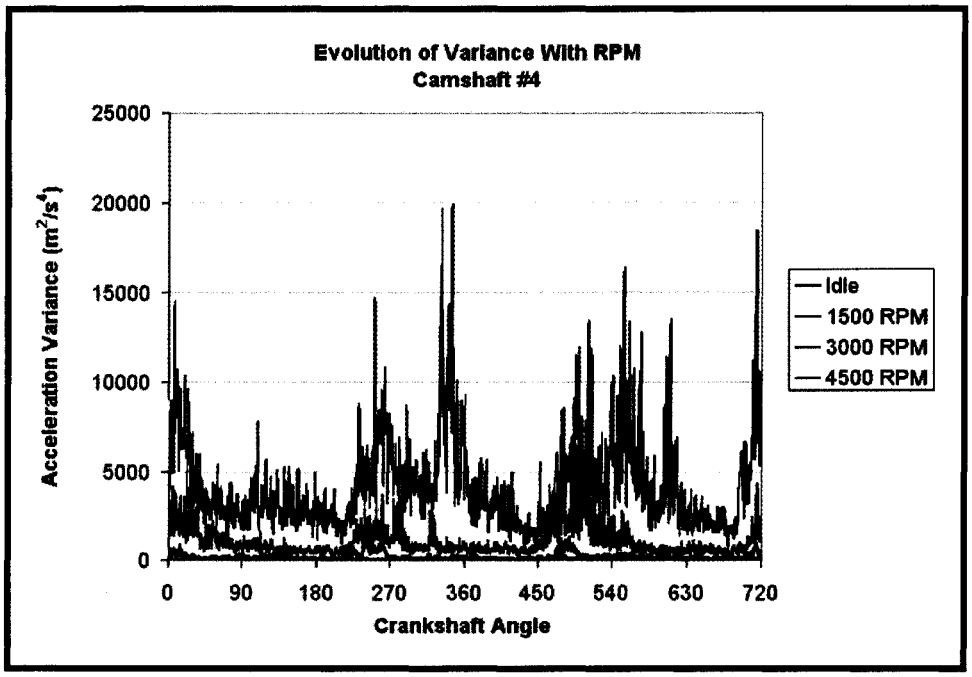

Figure C.4: Evolution of variance with RPM for camshaft #4.

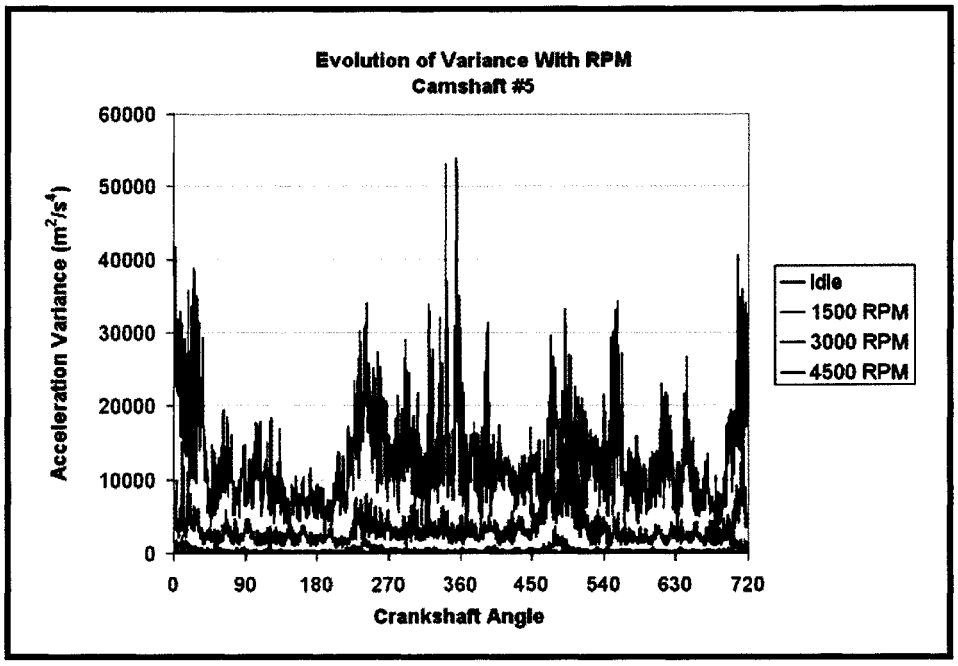

Figure C.5: Evolution of variance with RPM for camshaft #5.

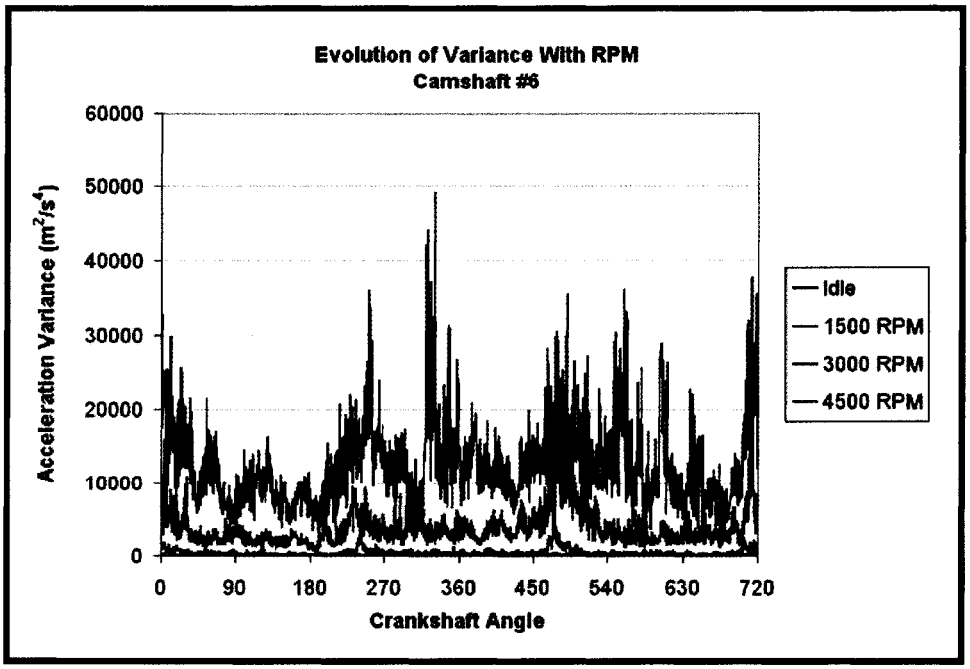

Figure C.6: Evolution of variance with engine RPM for camshaft #6.

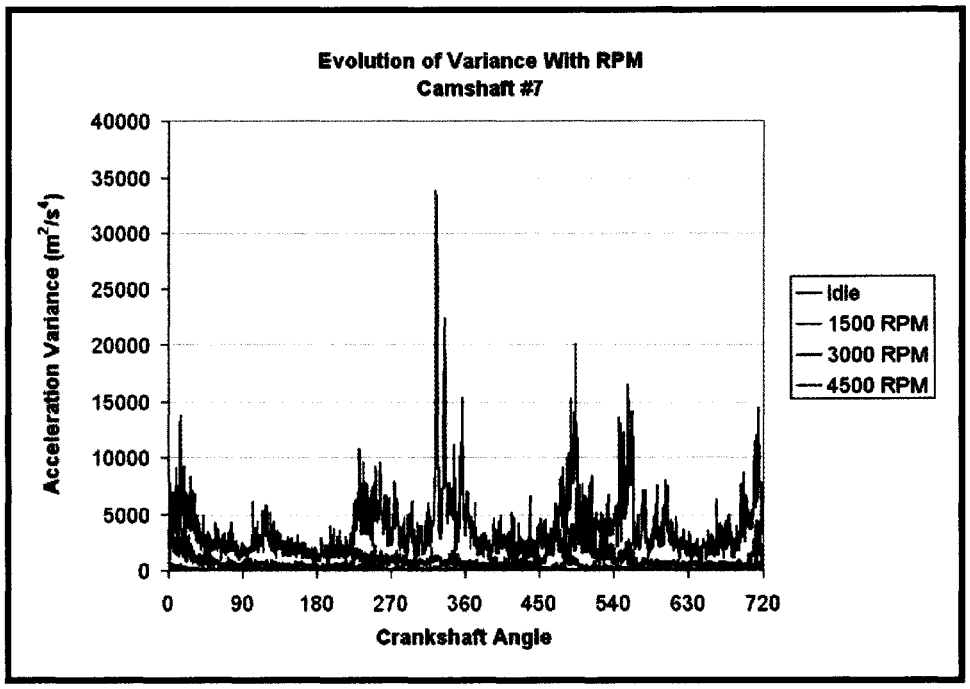

Figure C.7: Evolution of variance with RPM for camshaft #7.

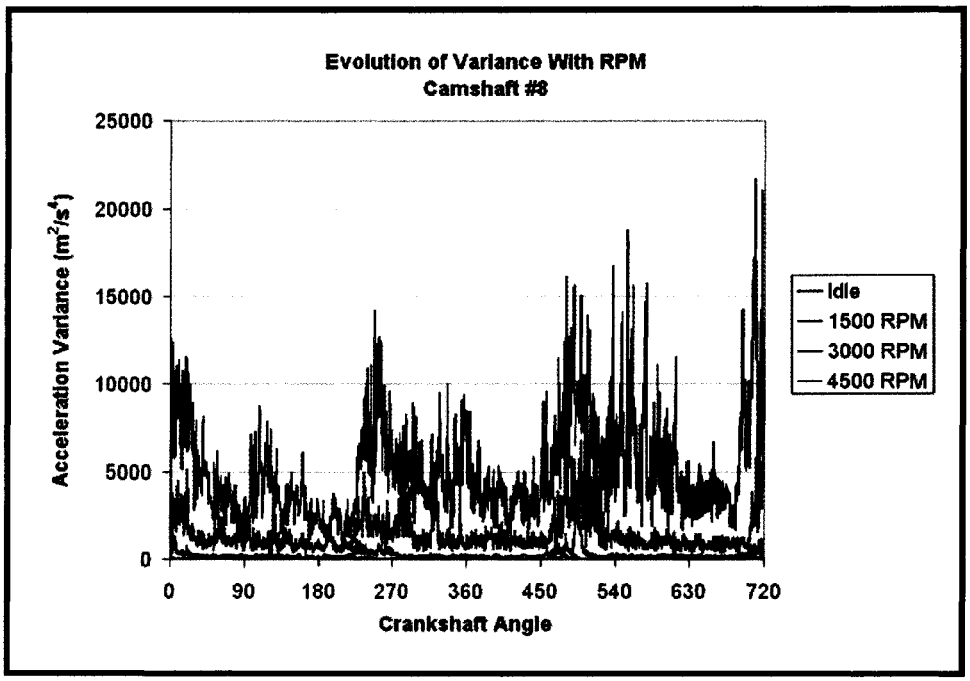

Figure C.8: Evolution of variance with RPM for camshaft #8.

APPENDIX D:

VARIANCE COMPARISON BY RPM

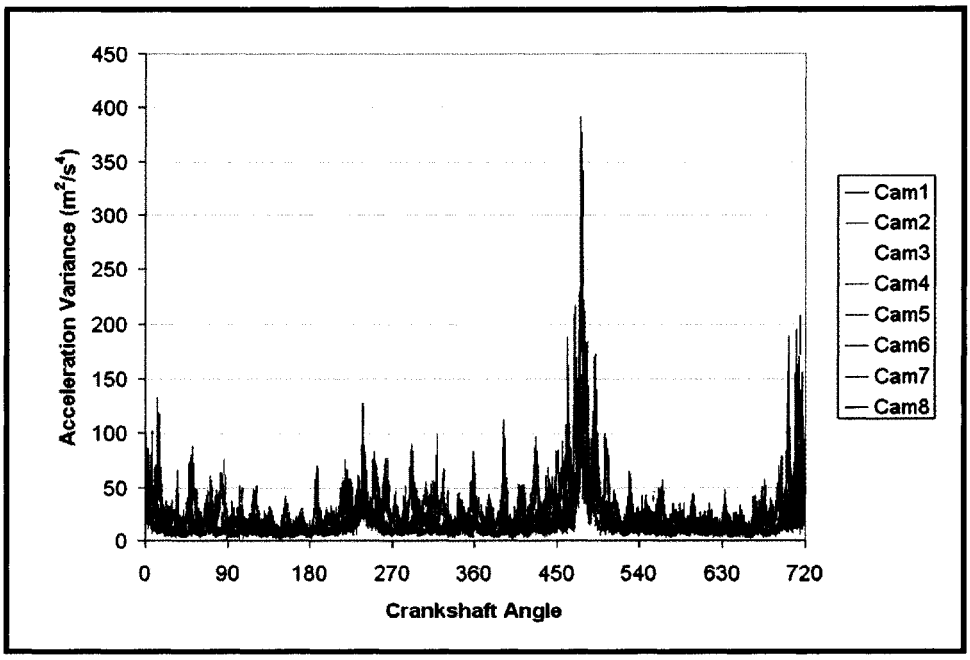

Figure D.1: Comparison of variance for all 8 cams at idle.

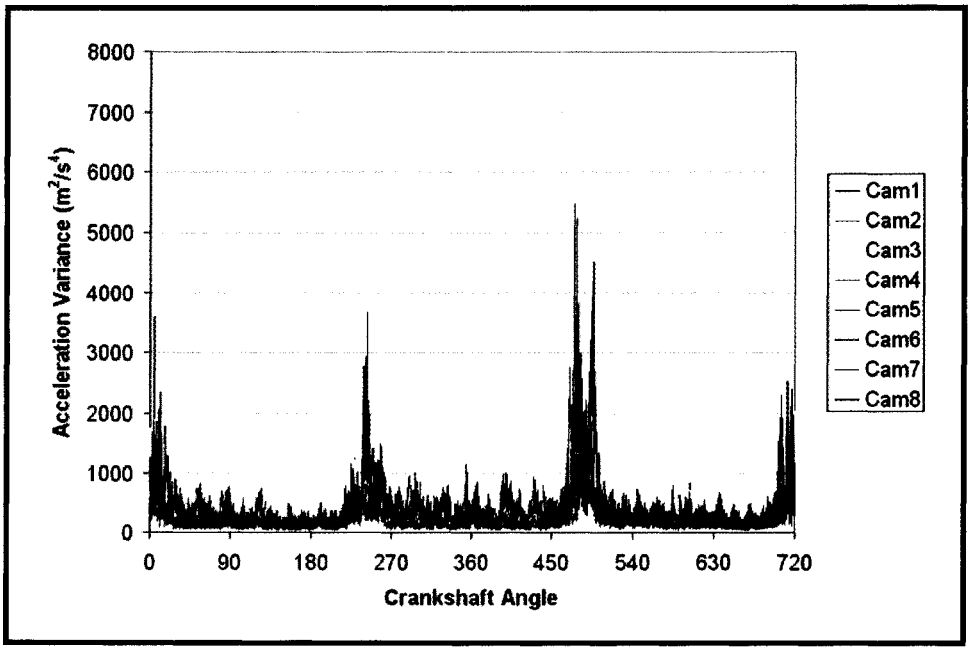

Figure D.2: Comparison of variance for all 8 cams at 1500 RPM.

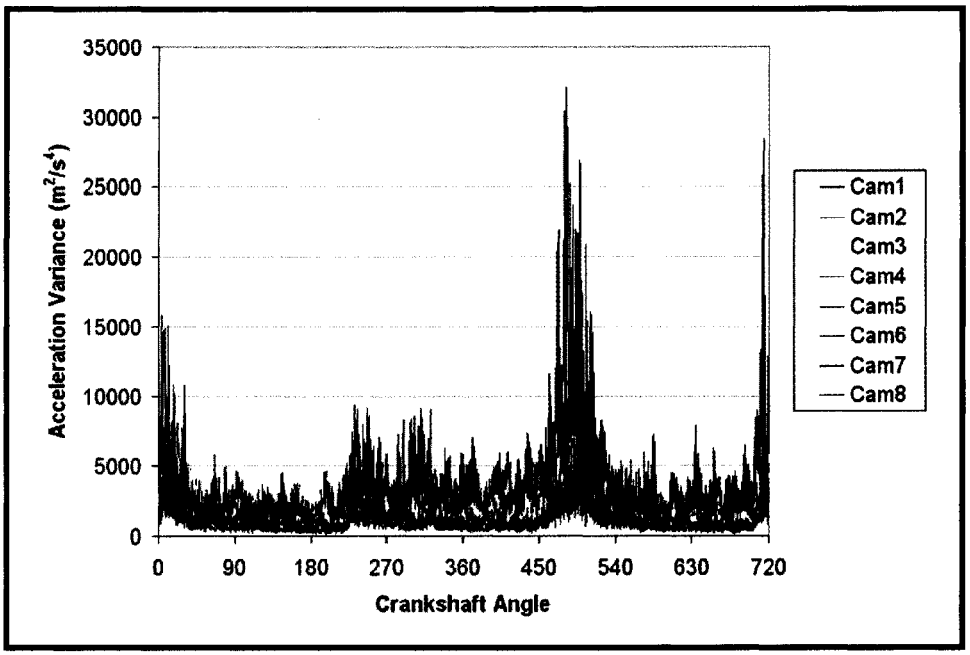

Figure D.3: Comparison of variance for all 8 cams at 3000 RPM.

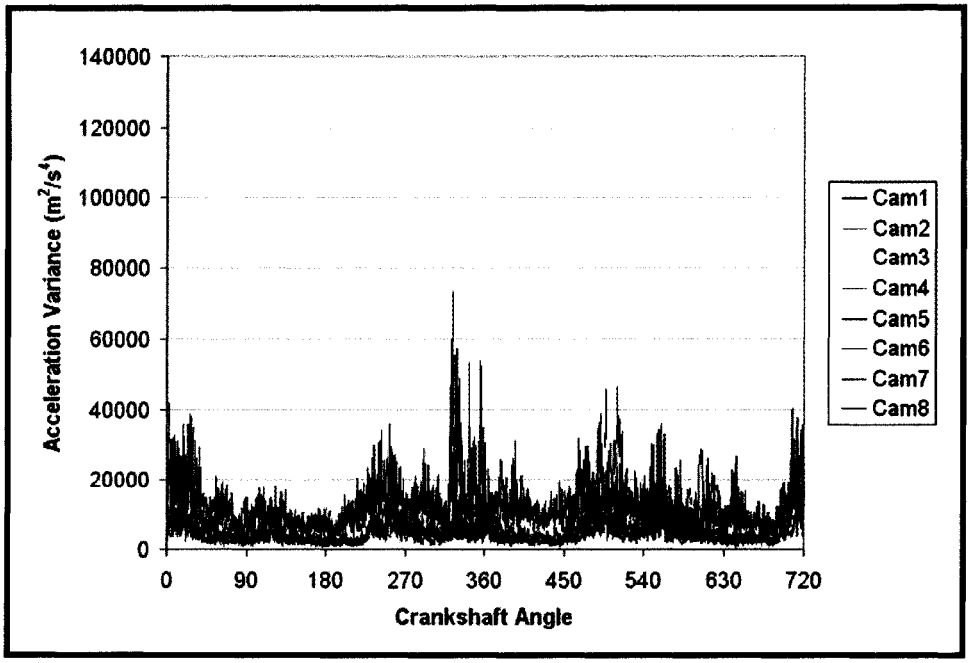

Figure D.4: Comparison of variance for all 8 cams at 4500 RPM.

APPENDIX E:

CAMSHAFT RPM-FREQUENCY COLOR MAPS

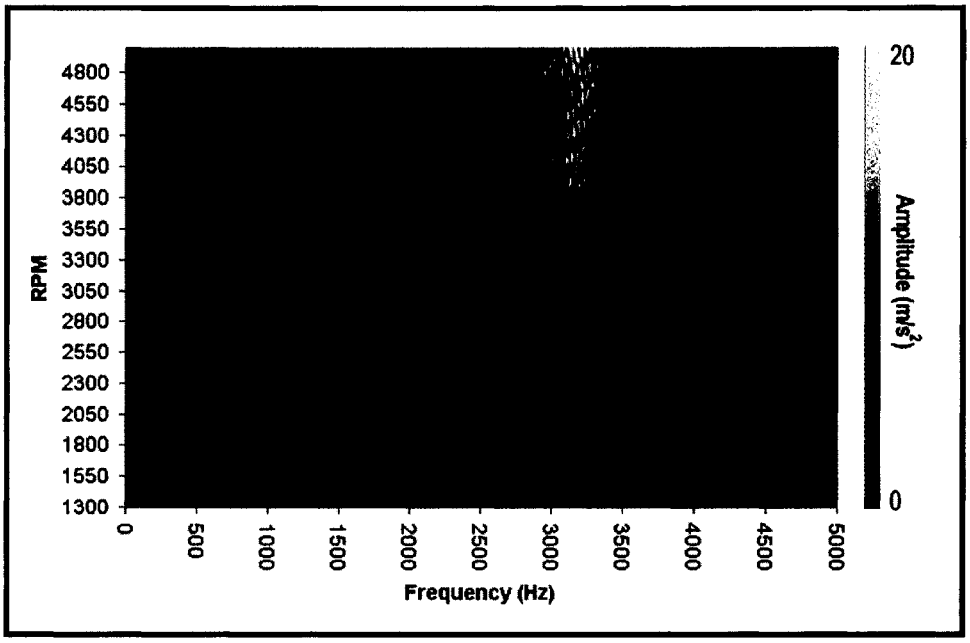

Figure E.1: Color map for camshaft #1.

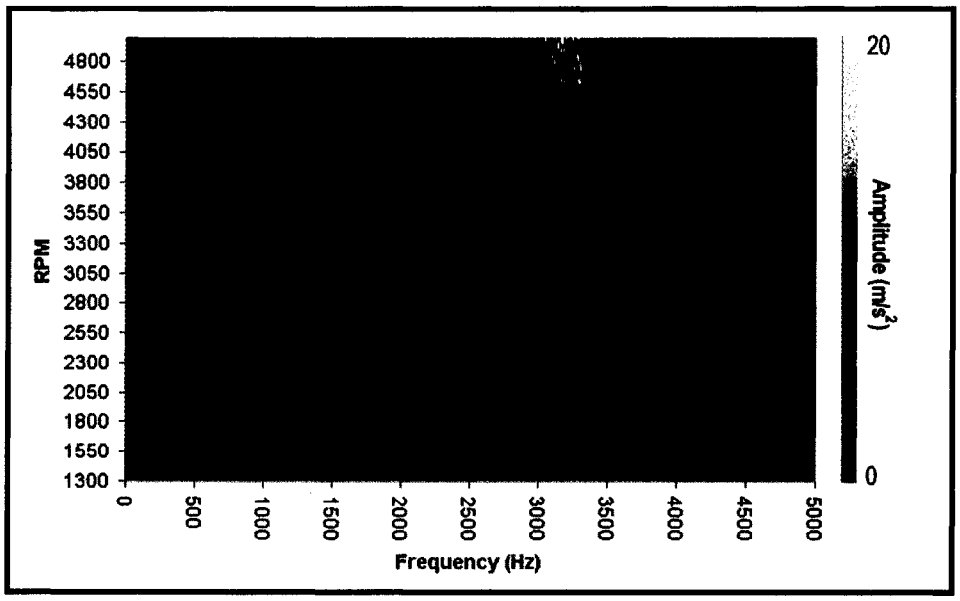

Figure E.2: Color map for camshaft #2.

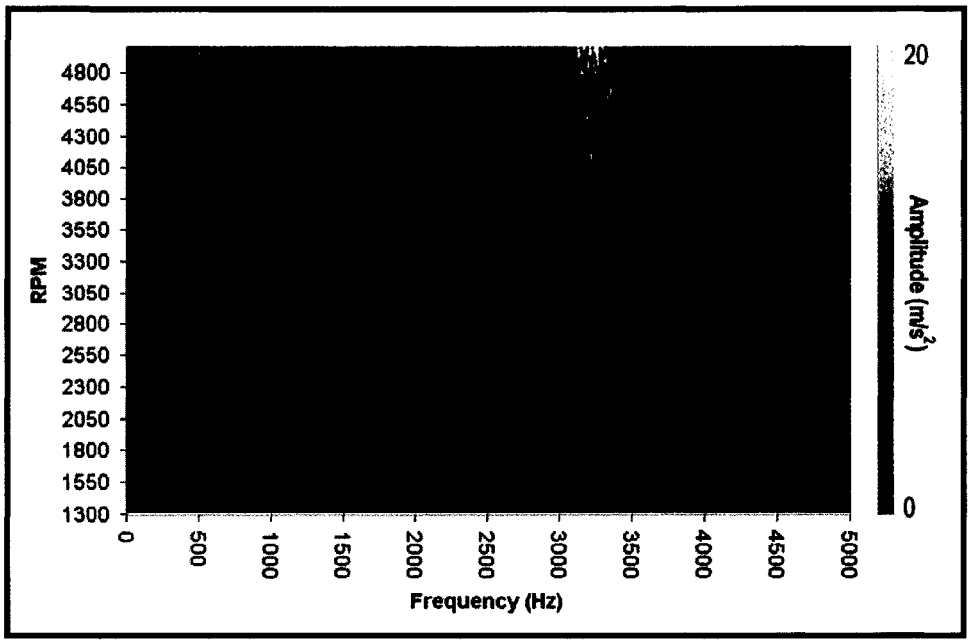

Figure E.3: Color map for camshaft #3.

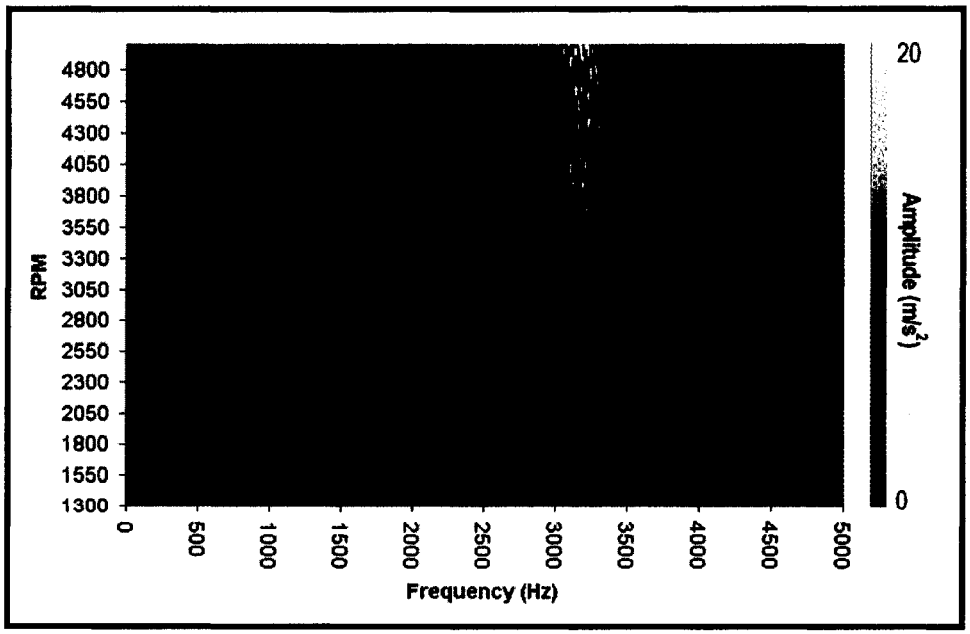

Figure E.4: Color map for camshaft #4.

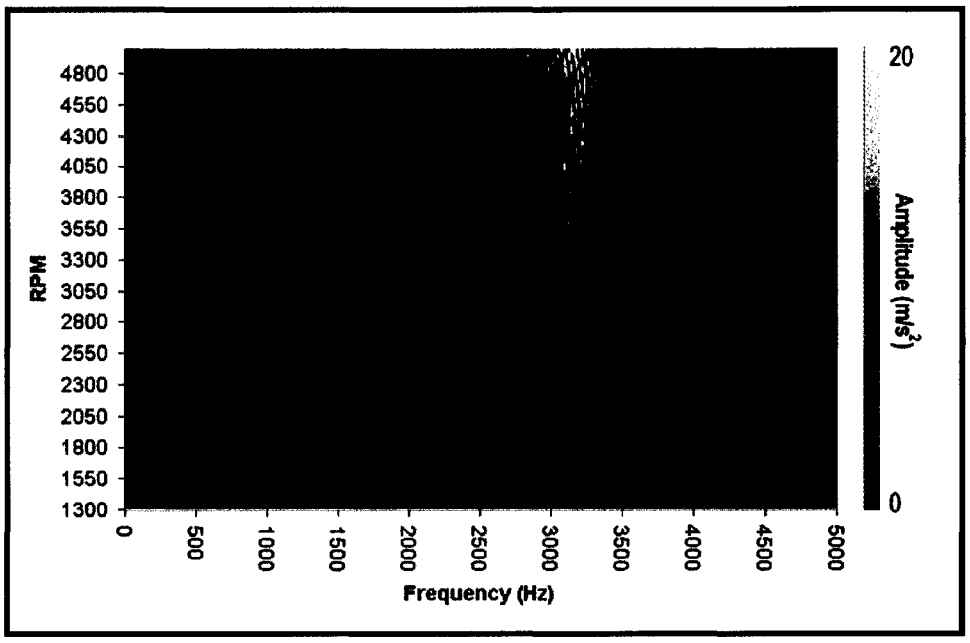

Figure E.5: Color map for camshaft #5.

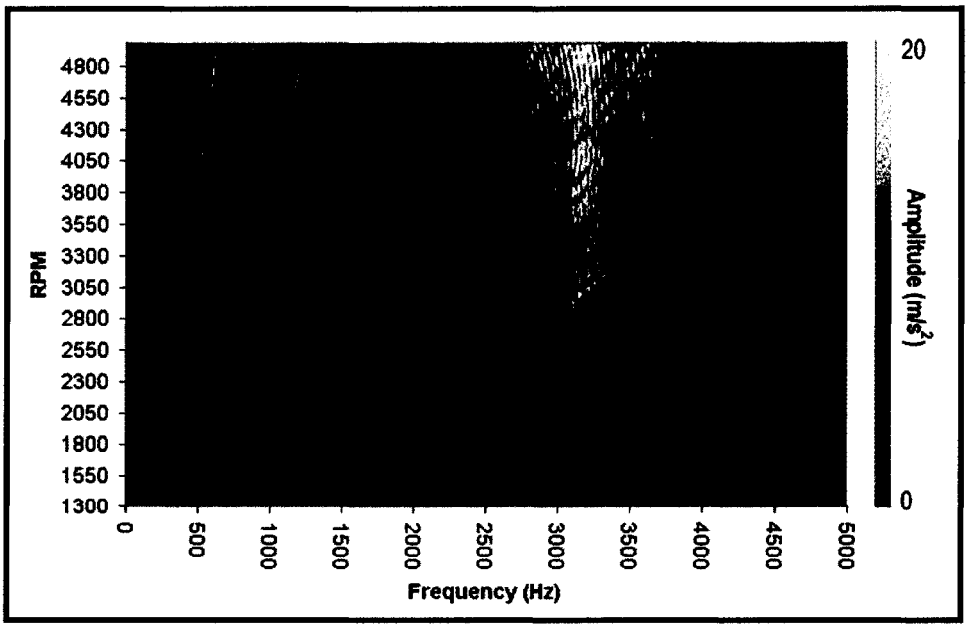

Figure E.6: Color map for camshaft #6.

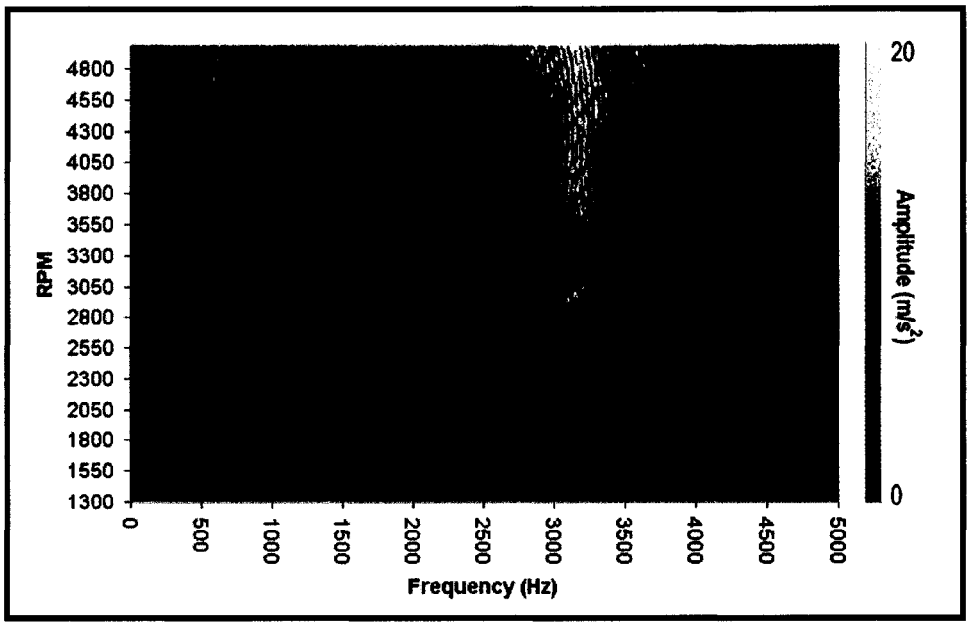

Figure E.7: Color map for camshaft #7.

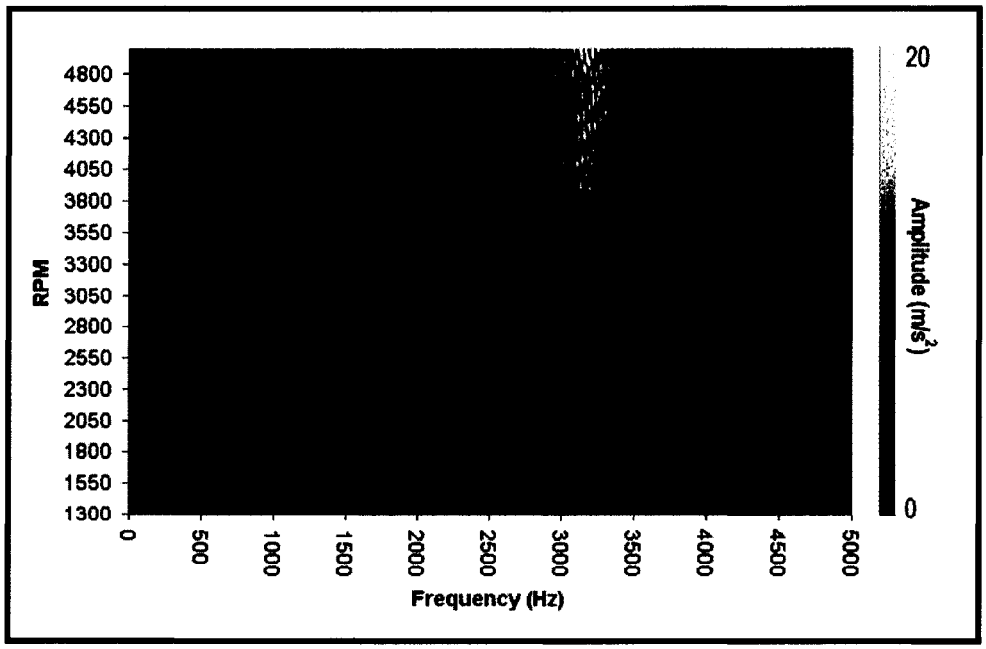

Figure E.8: Color map for camshaft #8.

APPENDIX F:

MAIN EFFECTS CALCULATIONS FOR MACHINING INPUTS

	A	B	C	D	E	RMS Acceleration 3000 - 4000 Hz		
	Wheel Vibration	Rotation Speed	Motor Vibration	Belt Tension	Clamp Pressure	1500 RPM	3000 RPM	4500 RPM
Cam 1	LOW	LOW	LOW	LOW	LOW			
Cam 2	LOW	HIGH	LOW	LOW	HIGH			
Cam 3	HIGH	LOW	HIGH	LOW	HIGH			
Cam 4	LOW	LOW	LOW	HIGH	HIGH			
Cam 5	HIGH	HIGH	LOW	HIGH	LOW			
Cam 6	HIGH	LOW	HIGH	HIGH	LOW			
Cam 7	HIGH	HIGH	HIGH	HIGH	HIGH			
Cam 8	LOW	HIGH	HIGH	LOW	LOW			

Figure F.1: Chart summarizing the response of each camshaft.

Notation: $\overline{X}_{A+}$ = average response when factor A is HIGH.
$\overline{X}_{A-}$ = average response when factor A is LOW.
$\overline{X}_{A+} - \overline{X}_{A-}$ = "main effect" of factor A

F.1 Calculation of Main Effects for 1500 RPM

$$\overline{X}_{A+} - \overline{X}_{A-} = \frac{4.59+4.37+4.74+5.21}{4} - \frac{4.31+4.41+4.41+4.31}{4} = 0.37$$

$$\overline{X}_{B+} - \overline{X}_{B-} = \frac{4.41+4.37+5.21+4.31}{4} - \frac{4.31+4.59+4.41+4.74}{4} = 0.06$$

$$\overline{X}_{C+} - \overline{X}_{C-} = \frac{4.59+4.74+5.21+4.31}{4} - \frac{4.31+4.41+4.41+4.37}{4} = 0.34$$

$$\overline{X}_{D+} - \overline{X}_{D-} = \frac{4.41+4.37+4.74+5.21}{4} - \frac{4.31+4.41+4.59+4.31}{4} = 0.28$$

$$\overline{X}_{E+} - \overline{X}_{E-} = \frac{4.41+4.59+4.41+5.21}{4} - \frac{4.31+4.37+4.74+4.31}{4} = 0.22$$

F.2 Calculation of Main Effects For 3000 RPM

$$\overline{X}_{A+} - \overline{X}_{A-} = \frac{18.4+18.14+23.72+23.25}{4} - \frac{12.62+14.54+14.62+15.84}{4} = 6.47$$

$$\overline{X}_{B+} - \overline{X}_{B-} = \frac{14.54+18.14+23.25+15.84}{4} - \frac{12.62+18.40+14.62+23.72}{4} = 0.60$$

$$\overline{X}_{C+} - \overline{X}_{C-} = \frac{18.4+23.72+23.25+15.84}{4} - \frac{12.62+14.54+14.62+18.14}{4} = 5.32$$

$$\overline{X}_{D+} - \overline{X}_{D-} = \frac{14.62+18.14+23.72+23.25}{4} - \frac{12.62+14.54+18.40+15.84}{4} = 4.58$$

$$\overline{X}_{E+} - \overline{X}_{E-} = \frac{14.54+18.40+14.62+23.25}{4} - \frac{12.62+18.14+23.72+15.84}{4} = 0.12$$

F.3 Calculation of Main Effects For 4500 RPM

$$\overline{X}_{A+} - \overline{X}_{A-} = \frac{31.95+29.13+38.67+46.48}{4} - \frac{25.72+25.66+26.40+26.65}{4} = 10.45$$

$$\overline{X}_{B+} - \overline{X}_{B-} = \frac{25.66+29.13+46.48+26.65}{4} - \frac{25.72+31.95+26.40+38.67}{4} = 1.29$$

$$\overline{X}_{C+} - \overline{X}_{C-} = \frac{31.95+38.67+46.48+26.65}{4} - \frac{25.72+25.66+26.40+29.13}{4} = 9.21$$

$$\overline{X}_{D+} - \overline{X}_{D-} = \frac{26.40+29.13+38.67+46.48}{4} - \frac{25.72+25.66+31.95+26.65}{4} = 7.675$$

$$\overline{X}_{E+} - \overline{X}_{E-} = \frac{25.66+31.95+26.40+46.48}{4} - \frac{25.72+29.13+38.67+26.65}{4} = 2.58$$

VITA AUCTORIS

Matthew C. Daws was born on May 11, 1977 in Windsor, Ontario, Canada. He graduated from Sandwich Secondary School, LaSalle, Ontario in 1996. He enrolled in Engineering at the University of Windsor, Windsor, Ontario later that year, and received his Bachelor of Applied Science degree in mechanical engineering in the summer of 2000. Matthew is currently a candidate for the Masters of Applied science (M.A.Sc.) degree in mechanical engineering at the University of Windsor.